Tectonophysics 712–713 (2017) 396–414

Contents lists available at ScienceDirect

Tectonophysics

journal homepage: www.elsevier.com/locate/tecto

Backarc tectonism, volcanism, and mass wasting shape seafloor morphology in the Santorini-Christiana-Amorgos region of the Hellenic Volcanic Arc

Emilie E.E. Hooft [a,*], Paraskevi Nomikou [b], Douglas R. Toomey [a], Danai Lampridou [b], Claire Getz [a], Maria-Eleni Christopoulou [b], Daniel O'Hara [a], Gillean M. Arnoux [a], Miles Bodmer [a], Melissa Gray [c], Benjamin A. Heath [a], Brandon P. VanderBeek [a]

[a] Department of Earth Sciences, University of Oregon, Eugene, OR 97403, USA
[b] Department of Geology and Geoenvironment, National and Kapodistrian University of Athens, Panepistimioupoli Zografou, 15784 Athens, Greece
[c] Department of Earth Science and Engineering, Imperial College London, SW7 2AZ, United Kingdom

ARTICLE INFO

Article history:
Received 1 December 2016
Received in revised form 5 May 2017
Accepted 5 June 2017
Available online 7 June 2017

Keywords:
Seafloor morphology
Volcanic cones
Submarine landslides
Pyroclastic flows
Fault zones
Earthquakes

ABSTRACT

In subduction zone backarcs, extensional deformation and arc volcanism interact and these processes, together with mass wasting, shape the seafloor morphology. We present a new bathymetric map of the Santorini-Christiana-Amorgos backarc region of the Hellenic subduction zone by merging high-resolution multibeam swath data from the R/V *Langseth* PROTEUS seismic experiment with existing maps. The map together with Knudsen subbottom echosounding profiles reveal that recent tectonism, volcanism, and mass wasting are more prevalent in the Santorini-Amorgos region on the east side of Santorini than in the Christiana Basin on the west side. In the Santorini-Amorgos region, large normal faults form the Anydros and Anafi Basins. Where normal fault segments overlap, two nearby accommodation zones generate a relay ramp and the adjoining Anydros synclinal horst with associated complex faulting and elevated seismicity. The ongoing normal faulting in the Santorini-Amorgos region is accompanied by potentially tsunamigenic submarine landsliding; we identified a large submarine landslide along the Santorini-Amorgos Fault and a smaller landslide with an overlying debris chute along the Amorgos Fault. Volcanic activity is also focused in this eastern region along the Kolumbo lineament within the Anydros Basin. Within the Christiana Basin we discovered the Proteus Knoll and adjacent buried edifice. We suggest that this is an older volcanic edifice formed along the Hellenic Volcanic Arc between Santorini and Milos. Around Santorini itself, features formed during, and immediately after, the Late Bronze Age eruption dominate the seafloor morphology such as the northern strait and wrinkled seafloor pyroclastic flow deposits. This topography is continually reshaped at a smaller scale by ongoing mass wasting. We infer that the earthquake, volcanic, and tsunami activity of the Santorini-Amorgos region is a consequence of focused northwest-southeast extension as the southeastern Aegean moves away from the Attico-Cycladic complex in response to slab breakup and rollback.

1. Introduction

Continental extension occurs in a variety of tectonic settings and is typically accompanied by magmatic activity. In back arc settings, extension is induced in the overriding plate of a subduction system by slab roll back and may lead to the development of a back arc spreading center (Carlson & Melia, 1984; Uyeda & Kanamori, 1979). Backarc extension also appears to be associated with adjacent collisional zones that induce sharp rotation and curvature of the backarc region (Wallace et al., 2009). This is well expressed in the central and eastern Mediterranean where the African plate subducts northward beneath the European plate (Dewey et al., 1973; Ninkovich & Hays, 1972). In the eastern Mediterranean, backarc extension in the Aegean initiated with Arabia-Eurasia collision (36–25 Ma) and has accelerated due to tearing of the slab both in the east, near western Turkey, and in the west, near Corinth (Faccenna et al., 2006; Floyd et al., 2010; Jolivet et al., 2013; Karagianni & Papazachos, 2007; Makris, 1978; Papadopoulos et al., 1986; Papazachos & Delibasis, 1969; Royden & Papanikolaou, 2011; Shaw & Jackson, 2010; Tirel et al., 2004). A consequence is the ongoing high levels of seismicity in this region – the highest in Europe (Papazachos, 1980; Papazachos, 1990; Sachpazi et al., 2015).

* Corresponding author at: Department of Earth Sciences, 1272 University of Oregon, Eugene, OR 97403, USA.
E-mail address: emilie@uoregon.edu (E.E.E. Hooft).

http://dx.doi.org/10.1016/j.tecto.2017.06.005
0040-1951/

Within the extended Aegean backarc region arc magmatism has formed the Hellenic Volcanic Arc (Fig. 1) (Le Pichon & Angelier, 1979; McKenzie, 1972; Papazachos & Nolet, 1997; Spakman et al., 1988), which is currently located ~200 km behind the trench system. Volcanism began 3–4 Ma (Keller et al., 1990), including the catastrophic Late Bronze Age (LBA) eruption of Santorini and accompanying tsunami that destabilized civilizations in the eastern Mediterranean around 1610 BCE (Dominey-Howes, 2004; Friedrich, 2006; Marinatos, 1939; Papadopoulos, 2015). The seafloor geomorphology of the central Aegean backarc is shaped by the interactions between tectonism, volcanism, and mass wasting (Papazachos & Panagiotopoulos, 1993; Perissoratis, 1995; Piper & Perissoratis, 2003) and the geohazards from each of these processes include catastrophic earthquakes, volcanic eruptions, and tsunamis (Feuillet, 2013; Okal et al., 2009; Papadopoulos & Pavlides, 1992; Perissoratis & Papadopoulos, 1999).

Here we present a new high-resolution swath bathymetric map of a 130 km by 50 km region around Santorini volcano that was made using the US R/V *Marcus Langseth* during the recent PROTEUS marine-land seismic experiment in Nov-Dec 2015 (Fig. 1). This active source seismic experiment had the goal of mapping the deep magma plumbing system of the backarc volcano. Here we focus on the swath bathymetry and 3.5 kHz subbottom profiling data that were collected during seismic data acquisition. Though some areas of Santorini were recently mapped with high resolution (Johnston et al., 2015; Nomikou et al., 2012; Nomikou et al., 2013; Nomikou et al., 2014), the Christiana Basin and eastern portion of Santorini-Amorgos region were only covered by EMODNET bathymetry [http://www.emodnet-hydrography.eu], which has low resolution (250 m grid) and contains artifacts. The high resolution of the R/V *Langseth* multibeam swath maps compared to most existing maps around Santorini allow us to make a detailed geomorphologic interpretation. The new data allow us to: (i) identify the areas of most recent tectonic deformation and detail the geodynamic structure of the region between Santorini and Amorgos - the site of the largest Greek earthquake in the 20th century (Ambraseys, 1960; Brüstle et al., 2014; Galanopoulos, 1956; Papadopoulos & Pavlides, 1992); (ii) discover and describe new seafloor volcanic edifices along the Hellenic Volcanic Arc and along the NE extension of the Kolumbo volcanic chain; and (iii) locate and describe mass wasting features along the Amorgos and Santorini-Amorgos Faults as well as pyroclastic flow deposits on the flanks of Santorini volcano. We conclude that in the central Aegean backarc, slab breakup and rollback drive the interactions between arc volcanism and backarc extension, and that these processes, together with mass wasting, shape the seafloor morphology.

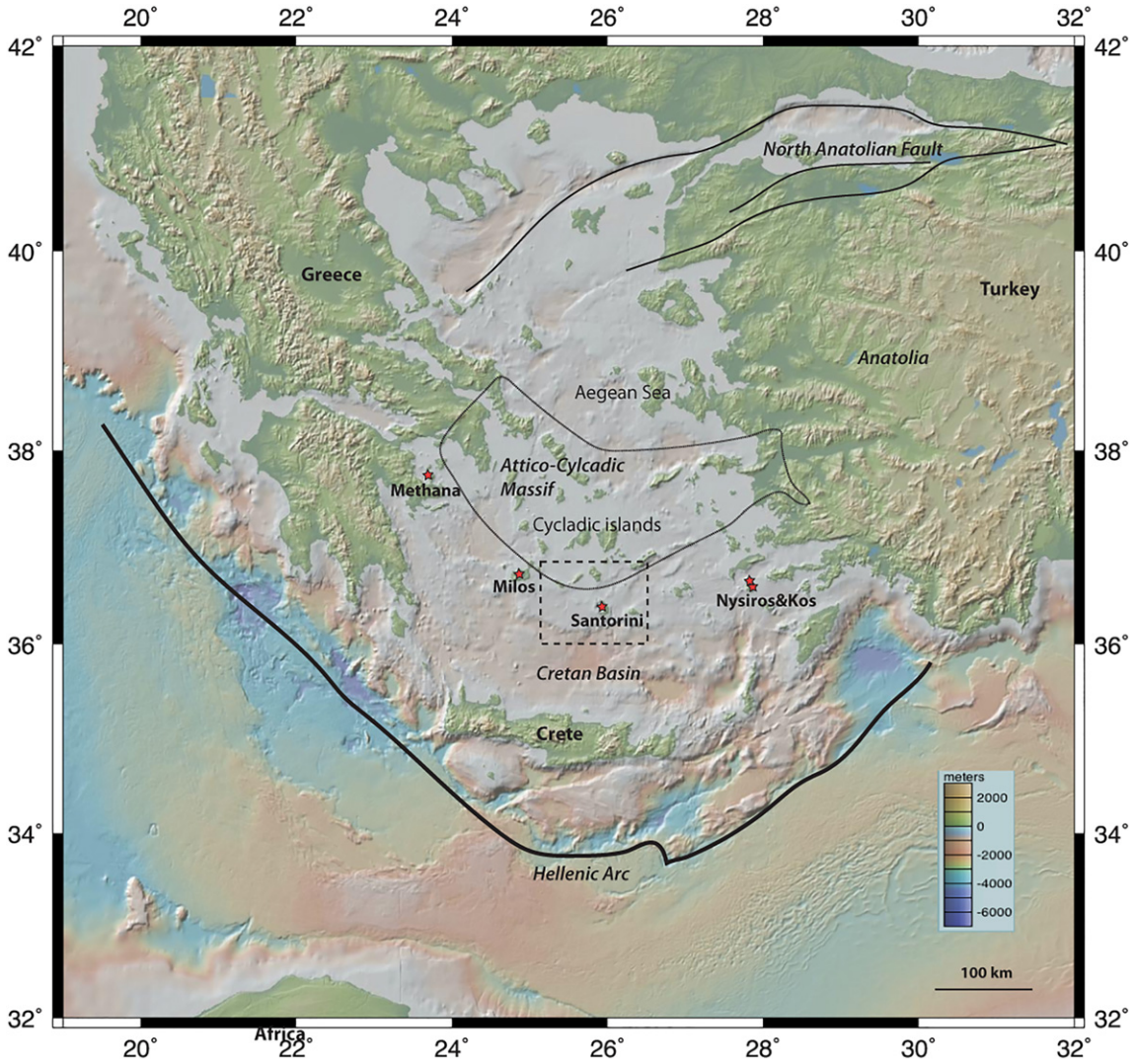

Fig. 1. Overview map showing Santorini at the center of the Hellenic Volcanic Arc (red stars at volcanic centers). Geographic and geologic features are shown in regular and italic text, respectively. The map was extracted using GeoMapApp [http://geomapapp.org]. The dashed box shows the region of the study area in Fig. 2. The dotted line surrounds the Attico-Cycladic Massif. (For interpretation of the references to color in this figure legend, the reader is referred to the web version of this article.)

2. Geologic setting

2.1. Tectonism

Extension of the southern Aegean has resulted in the substantial thinning of continental crust and the formation of horst and graben structures generating the Cycladic islands (Fig. 1) (Dermitzakis & Papanikolaou, 1981; Floyd et al., 2010; Jolivet et al., 2013; Karagianni & Papazachos, 2007; Le Pichon & Kreemer, 2010; Mascle & Martin, 1990; Papanikolaou, 2009; Papazachos, 1990; Royden & Papanikolaou, 2011; Sachpazi et al., 2015; Shaw & Jackson, 2010; Sodoudi et al., 2015; Tirel et al., 2004). The extensional deformation is driven by both westward extrusion of Anatolia along the North Anatolian Fault (McKenzie, 1972; Reilinger et al., 2010) and southward migration of the Hellenic Arc due to slab rollback (Le Pichon & Angelier, 1979). The area has a complex tectonic history as the geometry of slab retreat and fragmentation and collision has evolved through time (Jolivet et al., 2013; Papanikolaou & Royden, 2007; Taymaz et al., 2004).

The basement in the study area consists of metamorphic rocks of the Attico-Cylcadic complex that underwent compression in the early Cenozoic orogeny followed by major Miocene and younger extension (Papanikolaou, 2013; Piper & Perissoratis, 2003; Tirel et al., 2004). The extensively thinned Cretan Basin south of the study area and the Christiana Basin to the west of Santorini probably developed as a result of this Miocene extension (Fig. 2) (Endrun et al., 2008; Gautier et al., 1999; Piper & Perissoratis, 2003; Piper et al., 2007; Walcott & White, 1998). The large relief Christiana and Anafi Faults form the southern boundary of the study area with the Cretan Basin.

The eastern part of the study area, the Santorini-Amorgos region, is dominated by recent NW-SE extension (Bohnhoff et al., 2006; Floyd et al., 2010; Friederich et al., 2014; Nyst, 2004) and is thought to form a major structural boundary between the stable interior of the Attico-Cycladic complex and the eastern portion of the Hellenic Arc (Bohnhoff et al., 2006; McClusky et al., 2000; Nomikou et al., 2016b). In the Santorini-Amorgos region, recent NE-SW faults (initiated early Quaternary) with normal and strike-slip displacement overlie Pliocene E-W-normal faults that terminate against N-S transfer faults (Gautier & Brun, 1994; Perissoratis, 1995; Piper & Perissoratis, 2003; Piper et al., 2007; Tsapanos et al., 1994). The Anydros and Anafi Basins to the east of Santorini formed during the mid- to late-Quaternary (Piper & Perissoratis, 2003; Soukis & Papanikolaou, 2004). The Anydros Basin hosts a chain of underwater volcanic cones (Hübscher et al., 2015; Nomikou et al., 2012; Sakellariou et al., 2010) and is bounded by the Anydros and Ios Faults to the south and north, respectively. The Anafi Basin is bordered by large relief NE-SW oriented normal faults: the Santorini-Anafi Fault and the Santorini-Amorgos Fault on the south and north boundary, respectively. This basin has been the site of major subsidence during the last 0.2 Ma (Perissoratis & Papadopoulos, 1999; Piper & Perissoratis, 2003).

The largest 20th century earthquake in Greece (Ms = 7.4, Mw = 7.1) occurred between the islands of Santorini and Amorgos on July 9, 1956 (Makropoulos et al., 1989). The earthquake was accompanied by significant but localized tsunami runup (Ambraseys, 1960; Dominey-Howes et al., 2000; Galanopoulos, 1960; Okal et al., 2009). The earthquake epicenter has been variously located by different workers in the general area SW of the island of Amorgos at 25 to 45 km depth (Fig. 2b) (Brüstle et al., 2014; Comninakis & Papazachos, 1986; Okal et al., 2009; Papadopoulos & Pavlides, 1992) and was followed 13 min later by a second earthquake with a hypocenter located on the subduction interface beneath the island of Anafi (Brüstle et al., 2014). The dramatic elongated cliff along the southeast coast of the island of Amorgos is formed by a large normal fault (Stiros et al., 1994) with >1200 m of vertical relief from the cliff top to the seafloor of the adjacent Amorgos Basin. To the south of Amorgos it is less clear how this fault continues into the sea, yet understanding this structure is important given the uncertainty of the structure on which the 1956 deep normal faulting Amorgos earthquake occurred (Konstantinou, 2010; Okal et al., 2009). The localized tsunami that accompanied this earthquake was likely the result of mass wasting triggered by the earthquake (Okal et al., 2009). However, given the seismic station coverage and data quality of the time, and existing bathymetric maps, there continues to be uncertainty about the exact location of this earthquake and landslide (Brüstle et al., 2014; Okal et al., 2009). Delineating the active portions of this fault and any potential landslide regions is thus of societal impact.

2.2. Volcanism

Volcanism in the southern Cyclades is located along the Hellenic Volcanic Arc and consists of several volcano-tectonic clusters located (from west to east) at Methana, Milos, Santorini, Kos, and Nysiros (Fig. 1) (Fytikas et al., 1984; Keller et al., 1990; Pe-Piper & Piper, 2007). Volcanism at Santorini has been vigorous since its initiation ~400 kyr ago and major explosive eruptions have taken place in the last 220 kyr (Druitt, 2014; Druitt et al., 1999). Volcanism at Santorini interacts with existing tectonic structures (Feuillet, 2013; Nomikou et al., 2016b; Pe-Piper & Piper, 2007). The SE portion of Santorini itself is formed of a pre-existing horst of alpine basement (Heiken & McCoy, 1984), and initial volcanism at Christiana and Akrotiri on SW Santorini (Huijsmans et al., 1988; Seward et al., 1980) was likely focused by the fault on the western boundary of this alpine block (Feuillet, 2013). Santorini is a composite structure resulting from at least four caldera collapse events (Druitt & Francaviglia, 1992) and accompanying pyroclastic flows (Sigurdsson et al., 2006). The most recent Plinian eruption, the LBA eruption of 1610 BCE, formed the northern caldera basin (Druitt, 2014), which is bounded by steep cliffs and connected to the sea by three breaches (Nomikou et al., 2016a).

Volcanism is also focused along linear trends, the Kolumbo and Kameni lines that are aligned NE-SW in the same orientation as currently active faults (Fig. 1) (Druitt et al., 1999). Post-LBA eruptions led to the emplacement of the Palea- and Nea-Kameni islands at the center of the caldera (Fytikas et al., 1984; Johnston et al., 2015; Nomikou et al., 2014). To the northeast of Santorini, along the extension of the Kolumbo lineament, volcanism has formed the Kolumbo underwater volcano, which last erupted in 1650 CE, and the Kolumbo chain of smaller volcanic cones (Dimitriadis et al., 2009; Hübscher et al., 2015; Nomikou et al., 2012; Nomikou et al., 2014; Sakellariou et al., 2010).

2.3. Mass wasting

Mass wasting acts to reduce the relief created by tectonic and volcanic processes. Mass wasting can occur on a variety of scales from large-scale landsliding to slumping and rock flows within narrow debris chutes, to the movement of sediment laden turbidites over the seafloor and within seafloor channels (Masson et al., 2006; Mitchell et al., 2002). Mass wasting in the Christiana-Santorini-Amorgos region (i) has occurred during catastrophic events such as caldera forming eruptions (Nomikou et al., 2016a) and earthquake ground displacements (Okal et al., 2009); (ii) modifies over-steepened topography in an ongoing process (Croff Bell et al., 2013; Perissoratis & Papadopoulos, 1999); and (iii) may be connected to subaerial erosion resulting from precipitation (Mitchell et al., 2002).

3. Data and methods

Bathymetric data were acquired on-board the R/V *Marcus Langseth* using the Simrad Kongsberg EM122 12 kHz multibeam echo sounder. Data were processed using the MB-SYSTEM open-source software (http://www.mbari.org/mb-system) and merged with pre-existing data (Nomikou et al., 2012; Nomikou et al., 2013) (Fig. 2a). The EM122 multibeam bathymetry system has a maximum swath width up to 6 times the water depth depending on the sea state. The multibeam data processing included georeferencing using navigation

data, removal of erroneous beams, noise filtering, interpolation of missing data, and removal of rogue data points. Particular attention was paid to abrupt changes in seafloor topography due to steep relief at fault zones and volcanic edifices; these features were inspected and manually edited. To obtain complete coverage of the study area we merged the R/V *Langseth* map (Fig. S1) with existing bathymetry from Nomikou et al. (2012) and Nomikou et al. (2013) and topography for Santorini (Nomikou et al. 2014) (Fig. 2). The merged grid was generated

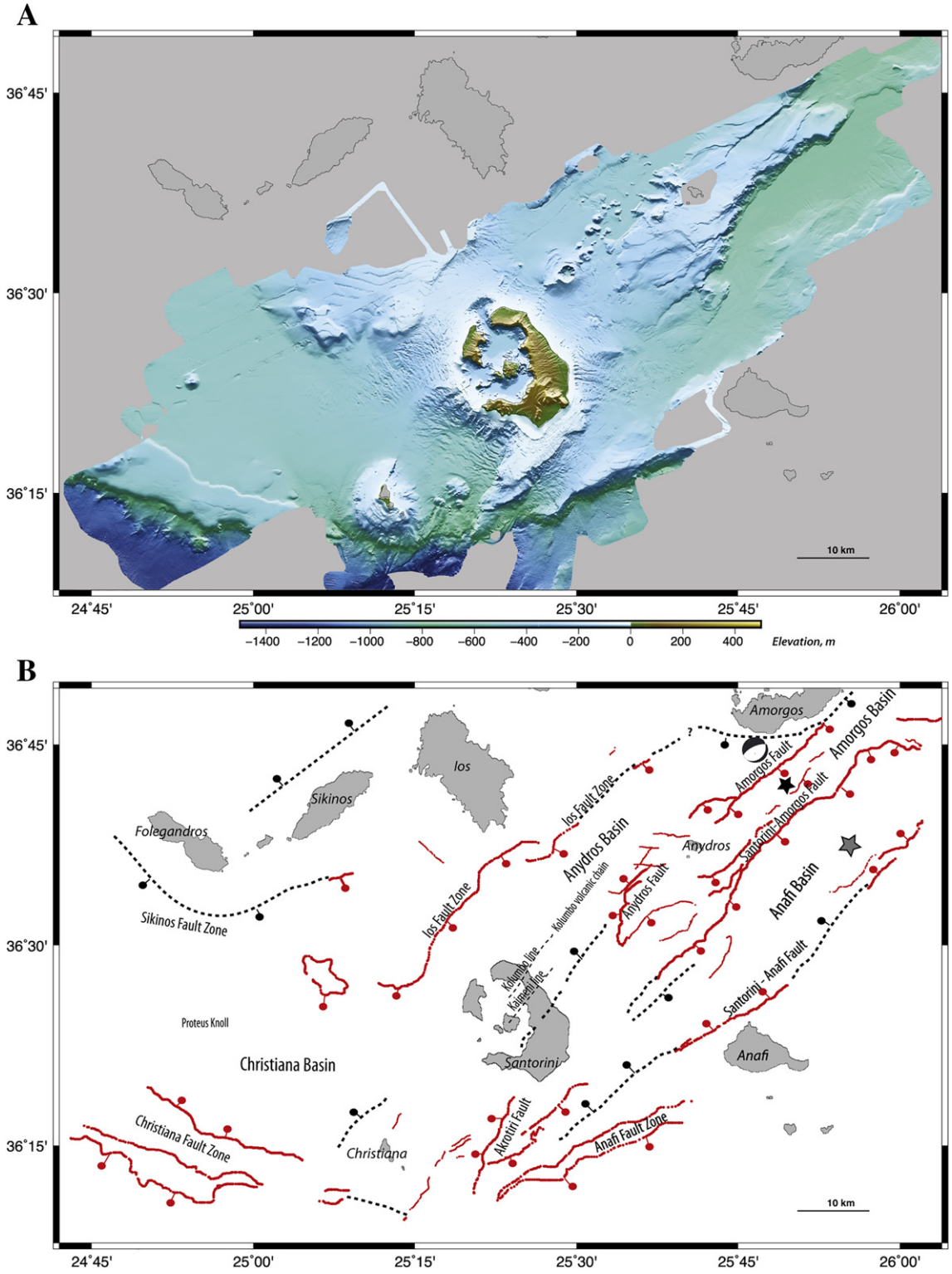

Fig. 2. a. Merged map gridded at 20 m and illuminated from the north. The R/V *Marcus Langseth* data was merged with maps from Nomikou et al. (2012) and Nomikou et al. (2014) and with Santorini topography from the Hellenic Military Geographical Service (HMGS). b. Schematic map showing major faults, basins, islands, and the epicentral locations of the 9 July 1956 Amorgos earthquake: focal mechanism by Okal et al. (2009), black star by Comninakis & Papazachos (1986), and grey star by Makropoulos et al. (1989). Red faults are from the maps in this paper; dashed lines are faults outlined in Hübscher et al. (2015), (Feuillet, 2013), and Nomikou et al. (2016b). Bars and dumbbell on the down-dropped side of the normal fault (hanging wall). (For interpretation of the references to color in this figure legend, the reader is referred to the web version of this article.)

at 20 m × 20 m and fills the gaps between the seismic lines, especially in shallow water, in the Santorini caldera, and includes the topography of Santorini island as well.

To image the character of the uppermost sediments, the R/V *Langseth* collected data with the Knudsen 3260 3.5 kHz echosounder. The Knudsen uses chirp hull mounted transducers and typically penetrates and reflects off the uppermost 100 m of sediments. Knudsen chirp data was converted to SEGY and visualized using the opendTect seismic interpretation software (www.opendtect.org).

4. Observations

The study area contains seafloor basins, horsts, faults, volcanic, and mass wasting features. To image and interpret the seafloor morphology

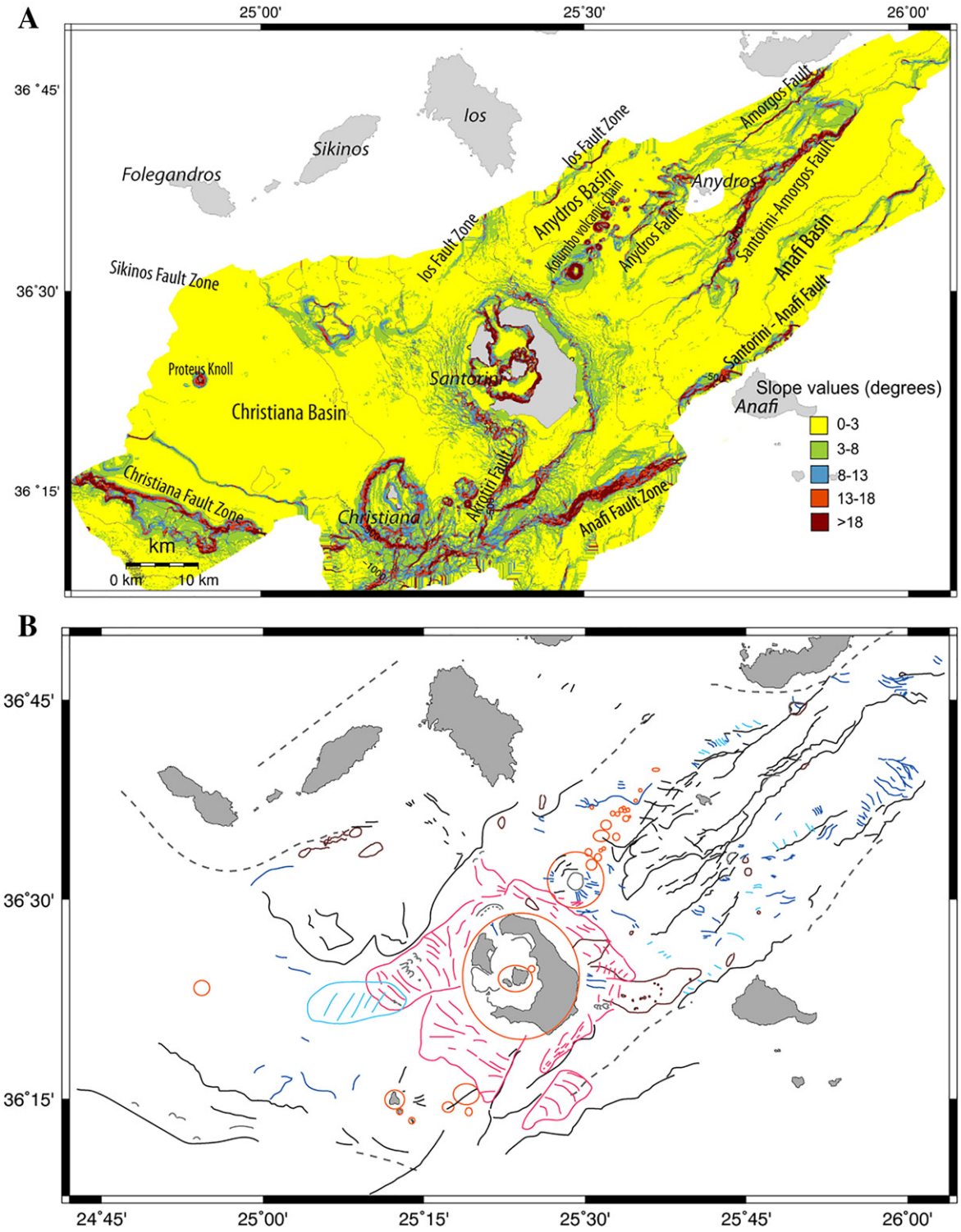

Fig. 3. (a) Map of slope magnitude calculated from the merged map (Fig. 2). (b) Interpretation of seafloor geomorphology from the merged map. Features outlined are: black = faults; grey dashed = established faults (Feuillet, 2013; Hübscher et al., 2015; Nomikou et al., 2016b); orange = volcanic edifices; red = wrinkled pyroclastic flow deposits; brown = landslide deposits; purple = mass wasting; dark blue = seafloor channels and debris chutes; light blue = seafloor ripples. (For interpretation of the references to color in this figure legend, the reader is referred to the web version of this article.)

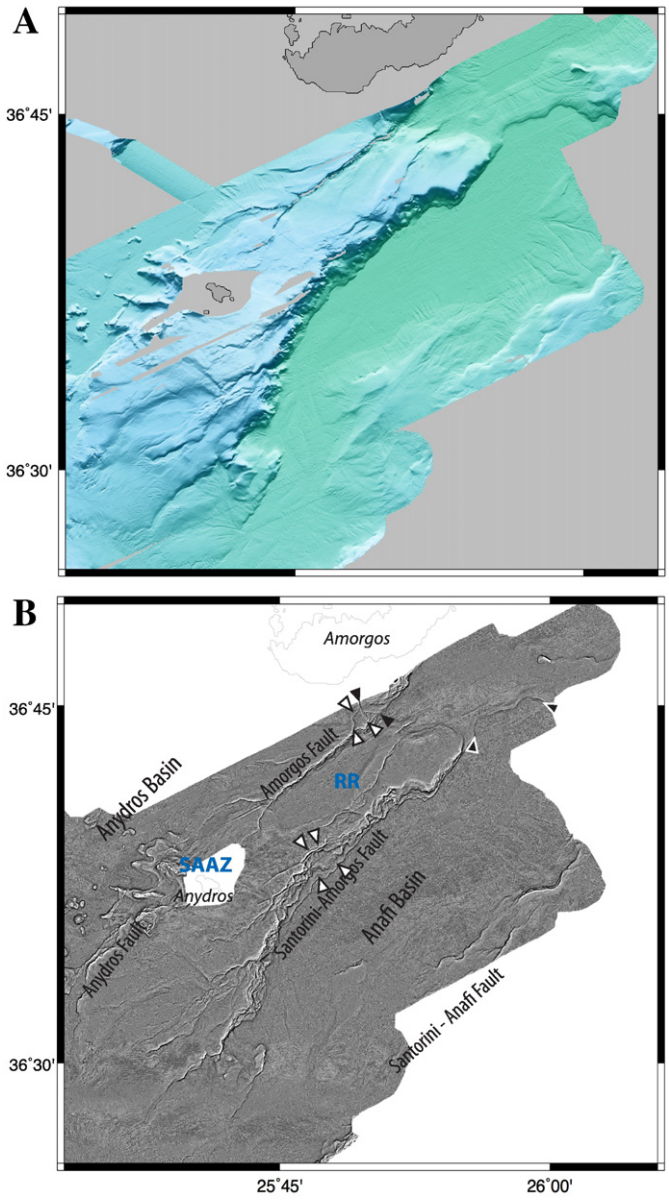

Fig. 4. Map of the Santorini-Amorgos and Amorgos Faults, the Anafi Basin, Anydros Horst and the Anydros Fault. (a) Bathymetry map illuminated from the north from the 20 m R/V *Langseth* data. Color scale as in Fig. 2. (b) Profile curvature from the merged map. The synthetic accommodation zone between the Santorini-Amorgos and Amorgos Faults produces a back-tilted relay ramp (RR) with secondary sub-parallel normal faults. The synclinal antithetic accommodation zone (SAAZ) between the Amorgos Fault and the Anydros Fault forms a high relief block within a regional syncline; this creates the Anydros island and is cut by numerous secondary faults. White arrows indicate the headwalls and toes of the large landslide on the Santorini-Amorgos Fault. A debris chute and associated runout (black arrows) overlays the east side of the smaller landslide (white arrows) on the Amorgos Fault. The NE end of the Anafi Basin is bounded by a sharp, low-relief normal fault with a perplexing curving morphology (black arrows with white outline).

we use standard morphometric computations such as slope magnitude (Fig. 3a), aspect, and profile curvature maps (Fig. S2). In this section we describe the identified faults, volcanic structures, and mass wasting features (Fig. 3b).

4.1. Faults and basins

We identify faults on the basis of their scarps, steep slopes, and quasi-linear nature, which give rise to consistent linear features in slope and aspect maps (Figs. 1–4, Figs. S1 & S2). We map the fault trace at the base of the scarp, especially in the case of a substantial vertical offset (e.g. the Santorini-Amorgos Fault Figs. 3 & 4). Some faults cross cut each other and the larger faults can be sinuous in map view (Fig. 4).

The coast of Amorgos is formed by a large fault, which we term the Amorgos Fault. We map the extension of the Amorgos Fault ~13 km to the southwest into the sea. The seafloor scarp of the Amorgos Fault is sharp and has normal down to the southeast motion and the size of the vertical relief diminishes to the south. Near its southwestern termination the fault splays and a normal fault strand extends to the west. The seafloor portion of the Amorgos Fault overlaps the parallel Santorini-Amorgos Fault that extends southwest toward Santorini.

For the first time, high-resolution bathymetry provides a detailed map of the Santorini-Amorgos Fault that forms the southern edge of the Anydros Horst and the northern boundary of the Anafi Basin (Fig. 4). The Santorini-Amorgos Fault has normal motion down to the southeast and is long (40 km) and steep with a large relief and a concave arcuate shape. Crossing the fault near its mid-point the seafloor drops from 250 to 725 m below sea level (bsl) (575 m relief) over a distance of 2.5 km, a slope of 20%. At the southwest end the fault approaches Santorini and the fault throw diminishes. Similar to the southern termination of the Amorgos Fault there are several EW trending fault strands that splay off to the west. These faults appear to form the southwest boundary of the Anydros Horst.

The Anydros Fault forms the northern boundary of the Anydros Horst and the southern boundary of the Anydros Basin (Figs. 4 & 5). It has opposite polarity of the Amorgos and Santorini-Amorgos Faults with normal motion down to the north. The seafloor expression of this fault is shorter (~20 km) and the vertical relief (200 m) is less than for the Santorini-Amorgos Fault.

The Anydros Basin is bounded to the north by the Ios Fault (Figs. 1–4). The Anydros Basin dips to the NE where the termination of the basin, near the island of Amorgos, remains unmapped. The southwestern termination of this basin is formed by the intersection of the Santorini volcanic edifice and a southward bend in the Ios Fault. Kolumbo underwater volcano lies within the Anydros Basin near Santorini and the Kolumbo volcanic chain extends off to the northeast (Nomikou et al., 2012) (Fig. 5).

The Anafi Basin is bounded to the north by the Santorini-Amorgos Fault, to the south by the Santorini-Anafi Fault, and at the southwest end by the Santorini volcanic edifice and the Anafi Fault zone along the northern edge of the Cretan Basin (Figs. 1–4). The floor of this basin dips down to the north toward the Amorgos Fault and also to the NE. At its NE termination the basin is bounded by a sharp low relief normal fault with a perplexing curving morphology (black arrows with white outline Fig. 4). Further mapping to the north and east will help elucidate structural relationships in that area.

The Christiana Fault system forms the western and southern boundary of the Christiana Basin and the northern boundary of the Cretan Basin (Figs. 1–3). It consists of a major normal fault with motion down to the south. This large fault scarp has experienced significant mass wasting. Parallel, and to the north, lies a smaller normal fault with motion down to the northeast thus forming a NW-SE oriented horst between the two faults. This is also the western boundary of the Christiana Basin, which is bounded to the north by the Sikinos and Ios Faults and to the east by the Santorini volcanic edifice (Fig. 1).

4.2. Seafloor volcanic constructs

The seafloor volcanic constructs (Figs. 2 & 3) are typically circular and steep sided (>13°). The Kolumbo volcanic chain consists of two adjacent parallel lines of volcanic cones that extend from the Kolumbo Seamount on the NE flank of Santorini to the NE (Fig. 5). We identify 25 volcanic cones compared to 19 identified previously by (Nomikou et al., 2012) – in fact their map covers almost all of the additional cones but the higher resolution of the new swath maps allows us to

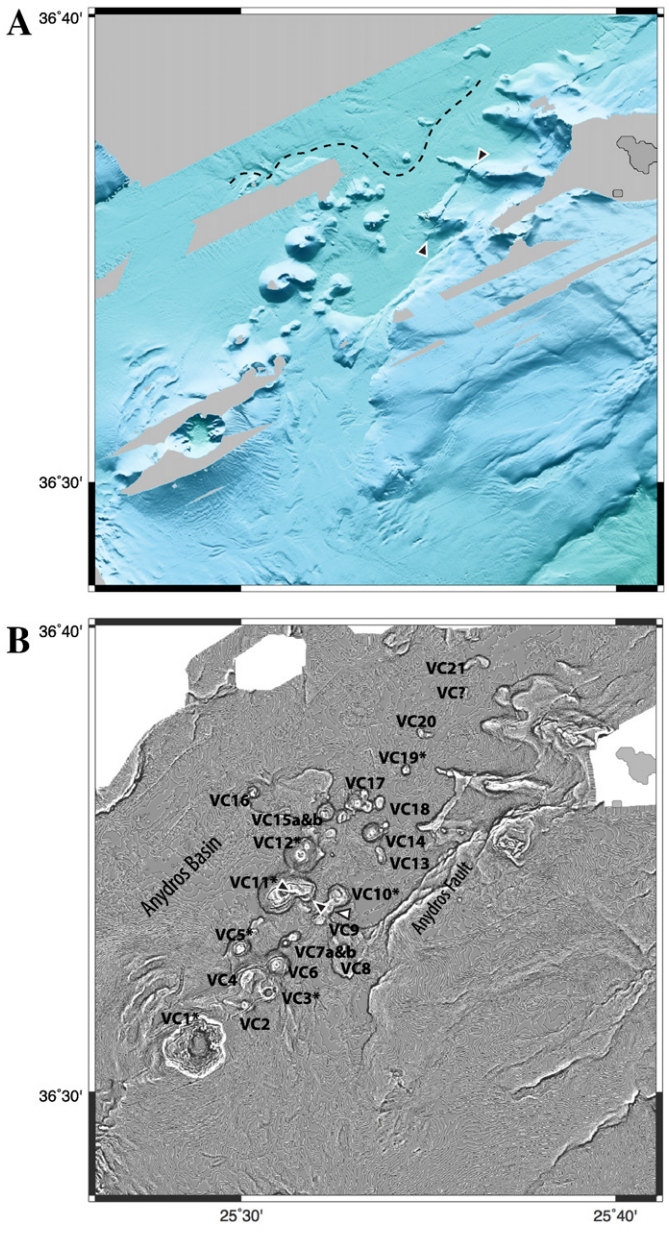

Fig. 5. Kolumbo Seamount and Kolumbo Volcanic Chain and the Anydros Fault. (a) Bathymetric map illuminated from the north from 20 m R/V *Langseth* data, color scale as in Fig. 2a. A wide seafloor channel (dashed line) winds around the northern cones in the Anydros Basin. Hinge faulting on the Anydros Fault is indicated with black arrows. (b) Profile curvature from the merged map. Volcanic cones are labeled following Nomikou et al. (2012). Asterisks indicate cones with a summit crater. A lava flow (white arrow) emanates from the base of cone VC10. Cone VC11 appears to be cut by a fault (black arrows).

identify them as part of the volcanic chain. The high resolution bathymetry resolves craters at the top of many cones (asteriks in Fig. 5). There is a lava flow identified on the basis of an elevated lobate region that emanates from cone VC10 (white arrow Fig. 5b). Lastly an E-W fault apparently dissects the eastern flank of the large cone VC11 (black arrows Fig. 5b).

In the northeastern portion of the Christiana Basin we discovered an unmapped seafloor knoll, which we name the Proteus Knoll (Fig. 6). This edifice rises 300 m above the surrounding seafloor (from 550 to 250 m bsl), is conical (diameter of 2.2 km) and its smooth sides are steep (15°). Knudsen profiles revealed the presence of a nearby edifice that is buried (Fig. 6b); it is located 1.5 km to the east-northeast of the Proteus Knoll. Deeper sediments onlap the sides of the buried edifice but at shallower depths they drape over it with diminishing topographic amplitude as the seafloor is approached; this indicates that marine sediments were deposited after the edifice formed (Fig. 6b). The slopes of the Proteus Knoll itself do not appear heavily sedimented and suggest a relatively young feature. However, the onlap of sediments, as well as slight pullup of the sediments where they abut the knoll, also show that sediments were likely deposited after the knoll formed (Fig. 6b).

To the east of Christiana there are three seafloor cones (Fig. 7b). The larger two cones are cut by faults that are sub-parallel to the NE-SW oriented Akrotiri normal fault indicating that extension associated with this fault may have facilitated magma movement to the surface.

4.3. Submarine pyroclastic flow deposits

Submarine pyroclastic flow deposits are identified morphologically by a widespread wrinkled surface surrounding Santorini volcano (Figs. 2, 3, 7 & 8). These wrinkles consist of terraces, steps, and blocky ridges that most likely result from downslope creep or slumping during, or just after, deposition of the pyroclastic flows (Sigurdsson et al., 2006). Profiles through the seafloor pyroclastic flow deposits show that on steeper seafloor topography the steps are wider spaced and have greater vertical offset; the steps range in size from 80 to 20 km by 800 to 500 m (Fig. 8a).

4.4. Mass wasting

Mass wasting features can be identified at various scales from landslides, to narrow debris chutes, to seafloor channels and ripples (Figs. 1–4) (Masson et al., 2006; Mitchell et al., 2002; Wright & Rathje, 2003). Landslides have headwall scarps with typically concave arcuate shapes, while the landslides toes are convex and lobate (Brüstle et al., 2014; Comninakis & Papazachos, 1986; Kvalstad et al., 2005; Okal et al., 2009; Papadopoulos & Pavlides, 1992).

The northern caldera entrance channel of Santorini has a clearly identifiable and dramatic headwall scarp (Figs. 8b & 9) (Nomikou et al., 2014; Nomikou et al., 2016a). It was recently shown that this northern strait was formed catastrophically as a retreating headwall by material backsliding into the Santorini caldera during the final phases of the LBA Plinian eruption and immediately afterwards (Nomikou et al., 2016a). Our high resolution maps (Fig. 9) show two subsidiary excavated regions at the top of the headwall indicative of ongoing secondary mass wasting and downslope movement of material at a smaller scale. Half way down the cliffs we identify an abrupt change in slope in the high resolution bathymetry revealing the presence of a stronger layer – likely a thick layer of lava flows (Fig. 9). A channel within the northern caldera entrance (Nomikou et al., 2016a) (red dashed box Fig. 9) is formed within recently deposited sediments (Johnston et al., 2015) and likely reflects the ongoing mass-wasting from the upper edge of the headwall scarp (Fig. 8b). After this channel passes through the narrowest portion of the caldera entrance the flow is no longer channelized and instead consists of 0.5–1 m scale ripples with wavelengths of 150 m until it reaches the northern Santorini caldera basin (Figs. 8b & 9).

We also image the large landslide on the SE flank of Santorini that was investigated in detail by Croff Bell et al. (2013) (Fig. 10). Numerous large blocks are clearly visible at its center (white arrows Fig. 10), while the seafloor along its margins is rippled – these are clearly seen in the slope magnitude maps (grey arrows Fig. 10). In the head region of the landslide we found narrow debris chutes that connect with the Santorini coast and within which there are small-scale ripples (black arrows in Fig. 10). To the north of this large landslide additional mass wasting blocks can be identified as well as another narrow debris chute. Interestingly, very few similar landslide blocks are found on the west flank of Santorini (Figs. 1–3).

We discovered a large submarine landslide along the Santorini-Amorgos Fault at 25°48′E and 36°38′N (Figs. 4 & 11). Characteristic features include the arcuate incision of the upper fault scarp at the head

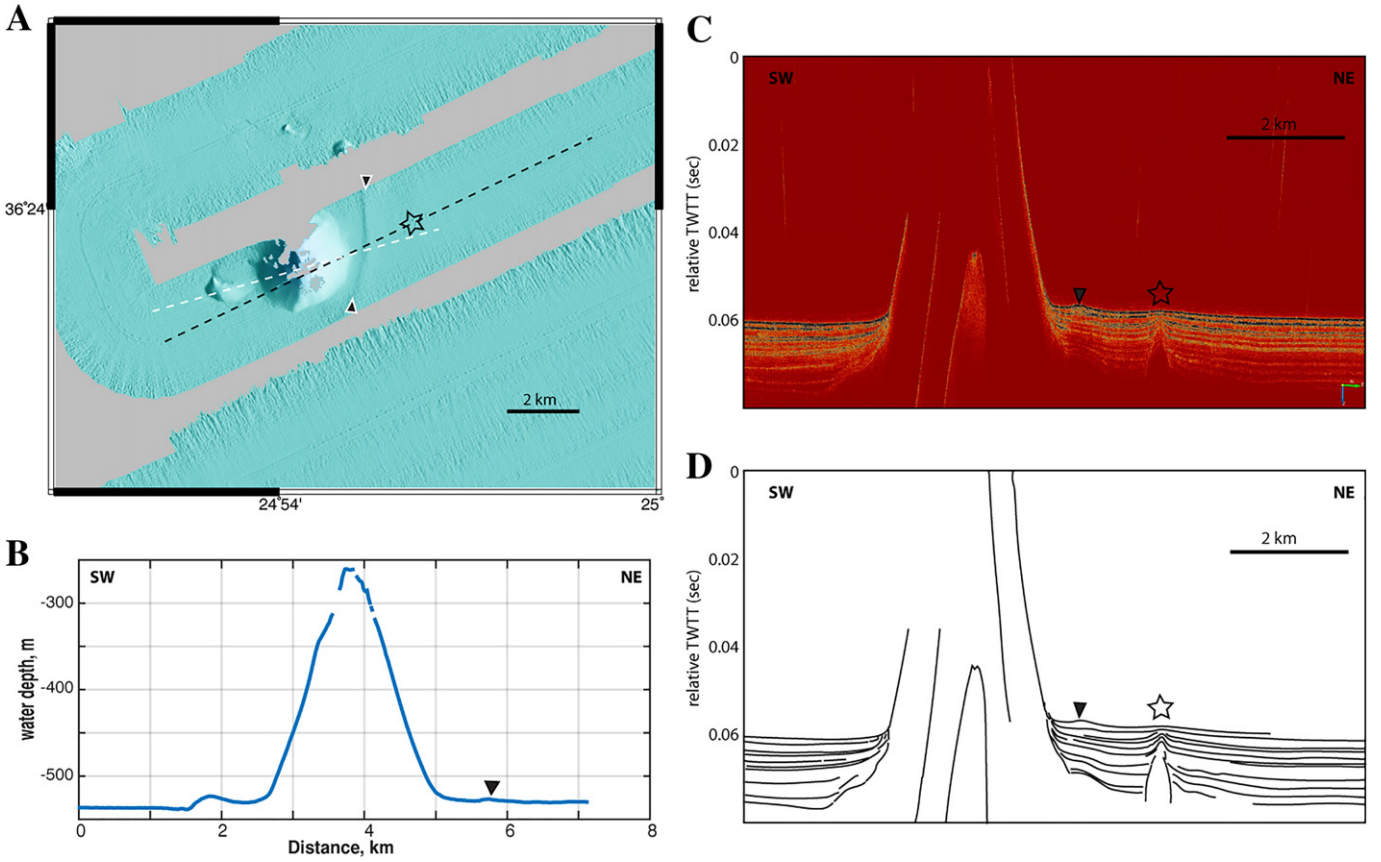

Fig. 6. Bathymetry and subbottom profiles of the newly discovered Proteus Knoll. (a) Bathymetry from the merged 20 m R/V *Langseth* data, color scale as in Fig. 2. Illumination from the east highlights a 1-m ridge of sediments (black arrows) curving around the eastern base of the edifice. (b) Bathymetric profile across the Proteus Knoll taken along the white dashed line in (a); slopes are 30%. (c) Knudsen subbottom echo-sounding profile taken along the dashed black line in (a). The time axis wraps twice on this display. An intrusion (star) can be seen in the sediments 2 km to the east. (d) Line drawing of the seismic facies in (c).

wall, the convex lobate shape at the base of the scarp, and broadening of the fault scarp itself (Fig. 11). The internal structure of this landslide consists of large lobes. Profiles through this landslide yield slopes at the headwall of 35%, while those within the toe are 13% (Fig. 11b). We estimate that the volume of this landslide is 1.3 km^3 by integrating the area under the profile through the landslide (Fig. 11b) and using a landslide width of 2.25 km (Fig. 11a).

On the seaward extension of the Amorgos Fault there is a smaller submarine landslide overlain by a narrow debris chute that appears to connect to a recently formed triangular bay on the Amorgos south coast (Figs. 4 & 12). This feature is located on the swath map that passes closest to the south coast of Amorgos at 25°50′E and 36°43′N. A clear arcuate headwall scarp and outward curving landslide foot are visible (white arrows Fig. 12). We estimate the volume of this landslide to be 0.3 km^3 by integrating the area under the profile through the landslide (Fig. 11b) and using a landslide width of 600 m (Fig. 11a). A narrow (150 m wide) debris channel joins the headwall scarp at its northeast end and the rougher seafloor topography of the more recent debris deposits fan out on top of, and along, the eastern margin of the landslide (black arrows Fig. 12). A sharply triangular bay is cut into the southern Amorgos coast about 2 km to the north and may be the source of the rocky debris material travelling down this chute (dashed line Fig. 12). At the base a narrow channel carries sediment-laden debris into the basin to the east and Knudsen profiles reveal a chaotic uppermost sedimentary cover indicative of mass wasting material.

Seafloor channels are formed by turbidity currents and sedimentary mass flows and can be identified particularly within the Anydros, Amorgos, and Anafi Basins (Fig. 13). These channels indicate the direction of recent movement of sediment-laden waters. Within the Anydros Basin a wide channel winds to the NE around the volcanic edifices of the Kolumbo lineament (Fig. 5). Within the Anafi Basin channels are directly downslope toward the base of the Santorini-Amorgos Fault and are relatively linear, likely a consequence of ongoing rapid subsidence controlling dense water flow (Fig. 13). Knudsen subbottom profiling shows that these channels formed very recently since their structure is only developed in the uppermost sedimentary layers (Fig. 14). Interestingly these channels appear to have formed on top of a preexisting updoming in the sediments. Seafloor channels are much less common in the Christiana Basin – likely a reflection of less dramatic bathymetric changes in recent time. The seafloor channels reflect the dominant direction of recent seafloor sediment movement and the numerous parallel channels perpendicular to the Santorini-Amorgos and Santorini-Anafi Faults indicate significant turbidity current displacement down tectonically generated gradients as the basins subside.

5. Discussion

The Amorgos-Anydros-Anafi region to the east of Santorini contains abundant evidence of recent deformation and volcanism with extreme changes in seafloor topography and accompanying mass wasting (Figs. 2 & 3). This is in contrast to the Christiana Basin west of Santorini, which appears to have experienced relatively little deformation in recent geologic time. These inferences are consistent with observations made by previous authors that there has been significant basin inversion, subsidence, and volcanism in this eastern region (Hübscher et al., 2015; Nomikou et al., 2012; Nomikou et al., 2013; Nomikou et al., 2016b; Perissoratis, 1995; Piper & Perissoratis, 2003; Sigurdsson et al., 2006). Below we use our new high-resolution merged swath map to discuss (i) the fault structures and interactions of the Anydros-Amorgos-Anafi region, (ii) the distribution of volcanism, (iii) the

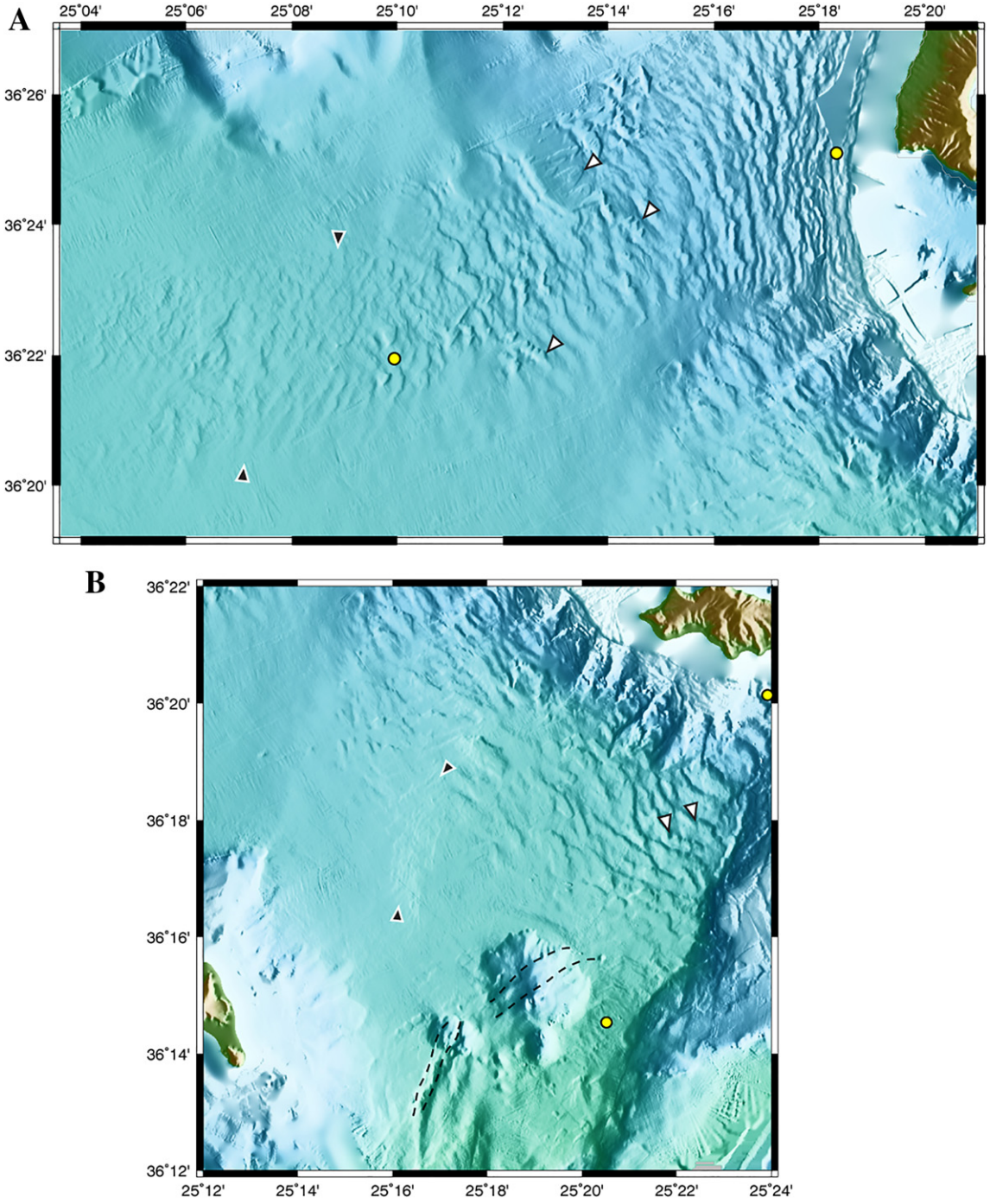

Fig. 7. Seafloor pyroclastic flow deposits on (a) the NW and (b) the SW flanks of Santorini. Bathymetric maps are from the merged map and are illuminated from the east, color scale as in Fig. 2. Yellow dots show the end points of profiles in Fig. 8a. (a) There is evidence of secondary mass wasting moving material downslope off ridges (white arrows). At the toe of the NW flank flow the seafloor wrinkles are overprinted by ripples oriented in the NE-SW direction (black arrows). (b) On the steep SW flank and canyon the wrinkles separate and are back-tilted by slumping (white arrows). Note that the smaller scale wrinkles (black arrows) rotate away from the topography of the Christiana edifice. Three volcanic cones are located east of the island of Christiana. The two larger ones appear cut by faults (dashed lines) that parallel the Akrotiri fault. (For interpretation of the references to color in this figure legend, the reader is referred to the web version of this article.)

seafloor pyroclastic flow deposits, and (iv) landslides on the Santorini-Amorgos and Amorgos Faults and their potential as tsunami sources.

5.1. Faults and accommodation zones

We delineate the detailed seafloor structure and accommodation zones of the active system of overlapping normal faults that consists of the NE-SW oriented Amorgos, Santorini-Amorgos, and Anydros Faults (Fig. 4). Topographic changes are dramatic and the fault system has accommodated much of the recent tectonic deformation in the area. Significantly, the structure of this fault system to the southwest of the island of Amorgos has remained uncertain due to a lack of detailed maps, in spite of the fact that this is the general location of the Ms. 7.4 1956 earthquake at 25 to 45 km depth (Brüstle et al., 2014; Comninakis & Papazachos, 1986; Okal et al., 2009; Papadopoulos & Pavlides, 1992). Furthermore the role of ongoing, low-level seismicity

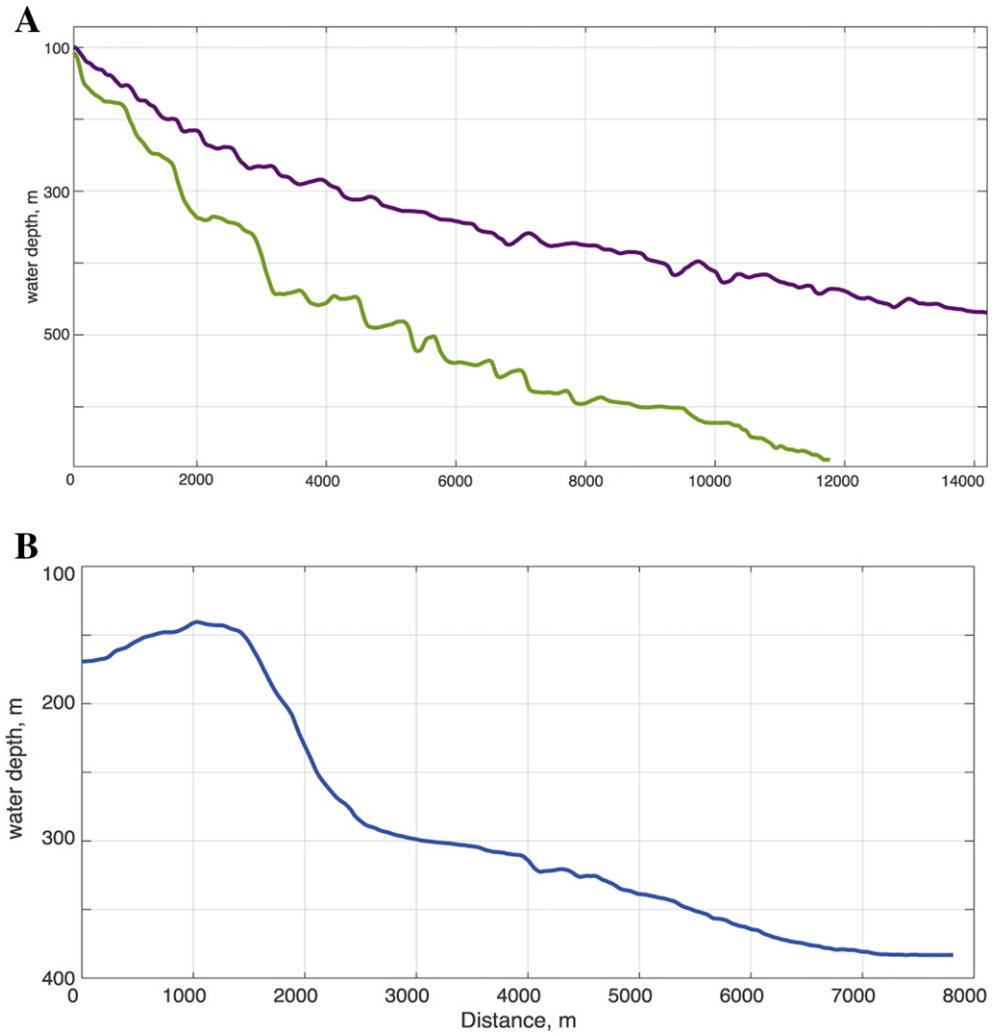

Fig. 8. Bathymetric profiles through (a) pyroclastic flows on the NW and SW flanks (purple and green, respectively) and (b) the northern caldera entrance channel. The end points of the profiles are shown by yellow dots in Figs. 7 and 9, respectively. (a) The pyroclastic flow deposits on steeper slopes have larger amplitude wrinkles that separate into distinct ridges. (b) Slopes of the headwall scarp of the northern caldera entrance channel are 20% and decrease through the channel into the northern caldera basin. (For interpretation of the references to color in this figure legend, the reader is referred to the web version of this article.)

near the island of Anydros within this system is intriguing (Bohnhoff et al., 2004; Bohnhoff et al., 2006; Dimitriadis et al., 2009; Friederich et al., 2014).

We have mapped the structure of the Amorgos Fault as it enters the sea to the south. Most current tectonic maps (Nomikou et al., 2016b) show the Amorgos Fault curving to the west around the southern end of Amorgos (Fig. 1) – a region that our maps do not cover. Our maps do clearly show that at least a branch of the Amorgos Fault continues into the sea 18 km directly to the SW with consistent normal motion down to the south. The vertical relief on the fault trace diminishes to the south and is very sharp suggesting recent deformation – it is possible that this fault surface has moved recently and thus may reflect surface rupture associated with the 1956 earthquake. Near its southern termination an E-W fault strand extends to west. The orientation of this fault strand may reflect reactivation of pre-existing EW oriented faults in the region (Perissoratis, 1995; Piper & Perissoratis, 2003). Given the various possible locations of the 1956 Amorgos earthquake (Fig. 1), it remains important to map how the Ios Fault at the north end of the Anydros Basin connects to the southern end of the island of Amorgos.

To the south deformation is transferred to the large Santorini-Amorgos Fault forming a large, left-stepping relay ramp (RR, Figs. 1, 4 & 15). The maps, as well as 2D MCS profiles (Hübscher et al., 2015; Nomikou et al., 2016b), show that both the Amorgos and Santorini-Amorgos Faults are normal faults with the same polarity - down to the SE. The faults overlap by 16 km and the relay ramp that lies between them is characteristically uplifted, back-tilted, and cut by a number of smaller normal faults that are subparallel to the main faults (Fig. 3). The curved shape of the Santorini-Amorgos Fault in map view (Figs. 4 & 11) is likely due to two factors: (i) breaching of pre-existing relay ramps thereby connecting smaller overlapping fault strands to form the larger composite fault (Bozkurt & Sözbilir, 2006; Fossen & Rotevatn, 2016) and (ii) mass wasting with arcuate incision of landslide headwalls in the scarp.

Structures around the island of Anydros consist of two kinds of fractures: E-W ridges that extend to the west from Anydros, which were cut by more recent NE-SW faults (Fig. 5). There is evidence of secondary hinge faulting within the hanging wall of the Anydros Fault. Where the Anydros Fault cuts the earlier E-W ridges their northwestern portions appear uplifted along secondary reverse faults (black arrows Fig. 5) (e.g., Fossen & Rotevatn, 2016; Sharp et al., 2000). The E-W ridges are not laterally offset indicating that there is no strike-slip component on the Anydros Fault. To the south the fault develops into a clear normal fault, the Anydros Fault. The Anydros Fault is offset down to the north into the Anydros Basin consistent with 2D MCS profiles (Nomikou et al., 2016b). Since the Anydros Basin tilts down to the northeast the vertical offset on the Anydros Fault must be less than that on the Ios and Amorgos Faults. At its southern end the seafloor expression of the

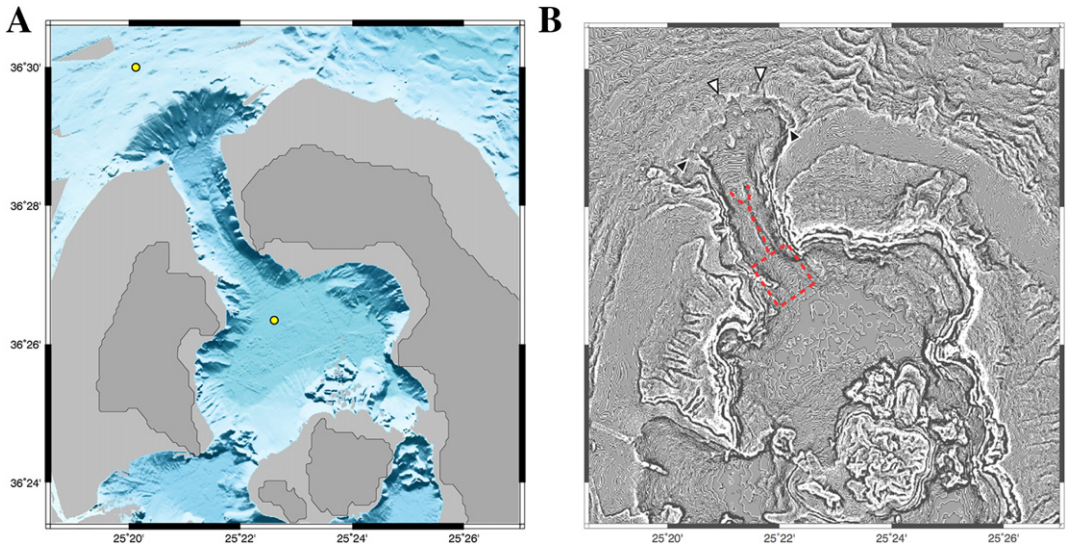

Fig. 9. Northern caldera entrance channel. (a) Bathymetric map illuminated from the north using the R/V *Langseth* data, color scale as in Fig. 2. Yellow dots show the end points of profiles in Fig. 8b. (b) Profile curvature from the merged map. Secondary mass wasting at the headwall scarp is shown with white arrows and black arrows show the more resistive layer half way down the headwall scarp. Flow in the northern part of the channel is confined to two seafloor channels that merge (red dashed lines), while the channel exhibits fine scale ripples across its width (dashed red box) as it opens up to the south into the northern caldera basin. (For interpretation of the references to color in this figure legend, the reader is referred to the web version of this article.)

Anydros Fault bends to the south and forms three convexly curved structures (Fig. 5). These curving fault structures connect to the SW trending fault strands at the southwest termination of the Amorgos Fault (Fig. 3).

Accommodation zones form due to the interaction at the terminations of segmented normal faults (Fig. 15). The interaction of the Santorini-Amorgos, the Amorgos, and the Anydros Faults form two adjoining accommodation zones that together generate the complex Anydros Horst (Fig. 4). The Santorini-Amorgos and Amorgos Faults overlap directly south of Amorgos forming a large, left-stepping relay ramp (Fig. 15). Since these two normal faults have the same polarity (dip in the same direction) this is known as a synthetic accommodation zone (Faulds & Varga, 1998; Rosendahl, 1987). The relay ramp, RR, connects the footwall of one fault to the hanging wall of the other fault and its internal deformation results in minor sub-parallel normal faults that form within the RR (Figs. 4 & 15). This geometry constructs the portion of the Anydros Horst located north of the island of Anydros.

Immediately to the south, around the island of Anydros and between the Santorini-Amorgos Fault and the Anydros Fault the polarity of the normal faults switches and is opposite giving rise to an antithetic accommodation zone (Faulds & Varga, 1998). Since the normal faults both dip outward this generates a synclinal antithetic accommodation zone [SAAZ in the terminology of Faulds & Varga (1998)]. Such SAAZs in the East African Rift and in the Basin and Range can form a local high relief block (high relief accommodation zone, HRAZ, in the terminology of Rosendahl (1987) that is regionally within a syncline. Thus the Anydros Horst is locally shallower than the adjacent Anafi and Anydros Basins and lifts Anydros above sea-level forming the small island (Figs. 4 & 15). However, on the regional scale the fault geometry forms a syncline and the Anydros Horst has lower elevation compared to the other Cycladic basement horsts in the area, which form the larger islands including Amorgos, Ios, and Anafi. Further characteristics of SAAZs are a greater abundance of subsidiary normal and oblique-slip faults (Faulds & Varga, 1998). This is reflected by the complex of smaller cross-cutting faults and the high level of seismicity around the Anydros Horst (Bohnhoff et al., 2006; Friederich et al., 2014).

Fig. 15 illustrates the interactions of the normal faults in the Santorini-Amorgos area. On a broad scale, opposing inward facing normal faults give rise to the Anydros and Anafi Basins. In detail, the interactions of the terminations of each fault segment explains the complex faulting structures seen in the RR and SAAZ regions around Anydros and perhaps also at the southwestern end of the Anydros Horst (Fig. 5).

5.2. Volcanism

It has been noted that the more recently formed volcanic features are located to the northeast of Santorini and are associated with the recent tectonic extensional deformation in this region (Fig. 1) (Feuillet, 2013). Specifically, the Kolumbo volcanic chain (Hübscher et al., 2015; Nomikou et al., 2012) in the Anydros Basin parallels the Anydros Fault (Fig. 5). This association of volcanism with tectonism is observed in other extensional terrains (e.g., Basin and Range) and is consistent with tectonic pathways through the lithosphere facilitating the ascent of magmas to the surface. It has also been suggested that there is an association between accommodation zones and volcanism and that young igneous intrusions may serve as rupture barriers to the lateral propagation of normal faults (Courtillot, 1982). While the volcanic edifices in the Santorini region appear to be associated with the intersection of faults with different orientations (Kokkalas & Aydin, 2013; Piper et al., 2007), the only evidence for volcanism specifically associated with the Anydros accommodation zone is the swarm-like character of microearthquakes in the Anydros area that have been interpreted to reflect fluid migration perhaps associated with magmatism (Bohnhoff et al., 2006).

A previous unknown seafloor knoll, the Proteus Knoll, and a nearby, buried edifice were discovered in the NW portion of the Christiana Basin (Fig. 6). The Proteus Knoll did not exist in the EMODNET seafloor bathymetric maps. The circular form, high magnetization, and steep sides of the knoll indicate a volcanic origin. The location of the knoll and adjacent buried edifice is enigmatic and it is unclear how old they are. Together the relatively unsedimented slopes of the knoll, as well as the adjacent sediment onlap, suggests that both are older features draped or covered by sedimentation (Fig. 6). The thinning and pullup of the sediments where they abut the knoll may result either from downslope movement of sediments or from the interaction of sediment laden bottom currents with the knoll. The presence of a 1-m sediment ridge to the east of the edifice and of deeper sediments to the west of the knoll than to the east suggest that a roughly east to west flowing seafloor current interacts with the knoll (Fig. 6). There are no identifiable seafloor faults in the proximity of the Proteus Knoll that might provide pathways

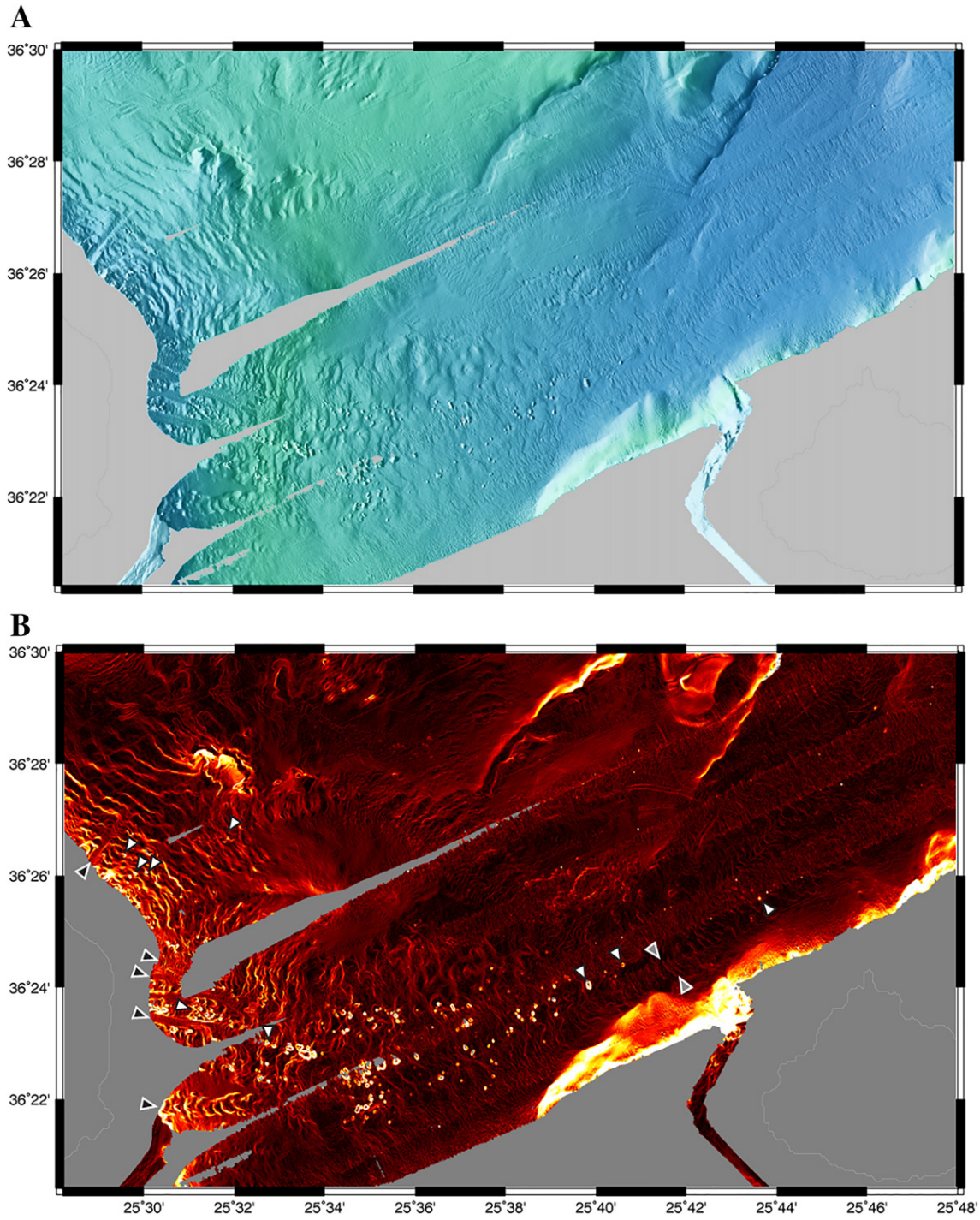

Fig. 10. Southeast Santorini submarine landslide. a) Bathymetric map illuminated from the northwest using the R/V *Langseth* data, color scale as in Fig. 2. (b) Map of slope magnitude from the R/V *Langseth* data indicating large blocks (white arrows), ripples (grey arrows) and debris chutes (black arrows); some of these features are located north of the main submarine landslide that was identified by Croff Bell et al. (2013).

to focus magmatism in this location. However, the knoll does lie on the curving line of the Hellenic Volcanic Arc that connects the volcanic centers of Santorini and Milos (Fig. 1). Consequently the Proteus Knoll is an intriguing target for further exploration.

5.3. Seafloor pyroclastic flow deposits

Santorini's flanks are covered with a thick layer of wrinkled or step-like morphology typical of submarine pyroclastic gravity flows (Figs. 2, 3, 7) (Carey & Sigurdsson, 2000; Carey et al., 1996). This massive or chaotic sedimentary layer was described and mapped by (Sigurdsson et al., 2006). These authors measure the thickness of this unit to average 29 m with a maximum of 80 m and a total bulk volume of 54.5 cubic kilometers or 41 cubic kilometers of dense rock equivalent. The wrinkled or step-like morphology likely results from downslope creep and slumping during and/or just after deposition. On steep slopes the terraces may detach and separate into distinct blocks (white arrows Fig. 7b) (Sigurdsson et al., 2006).

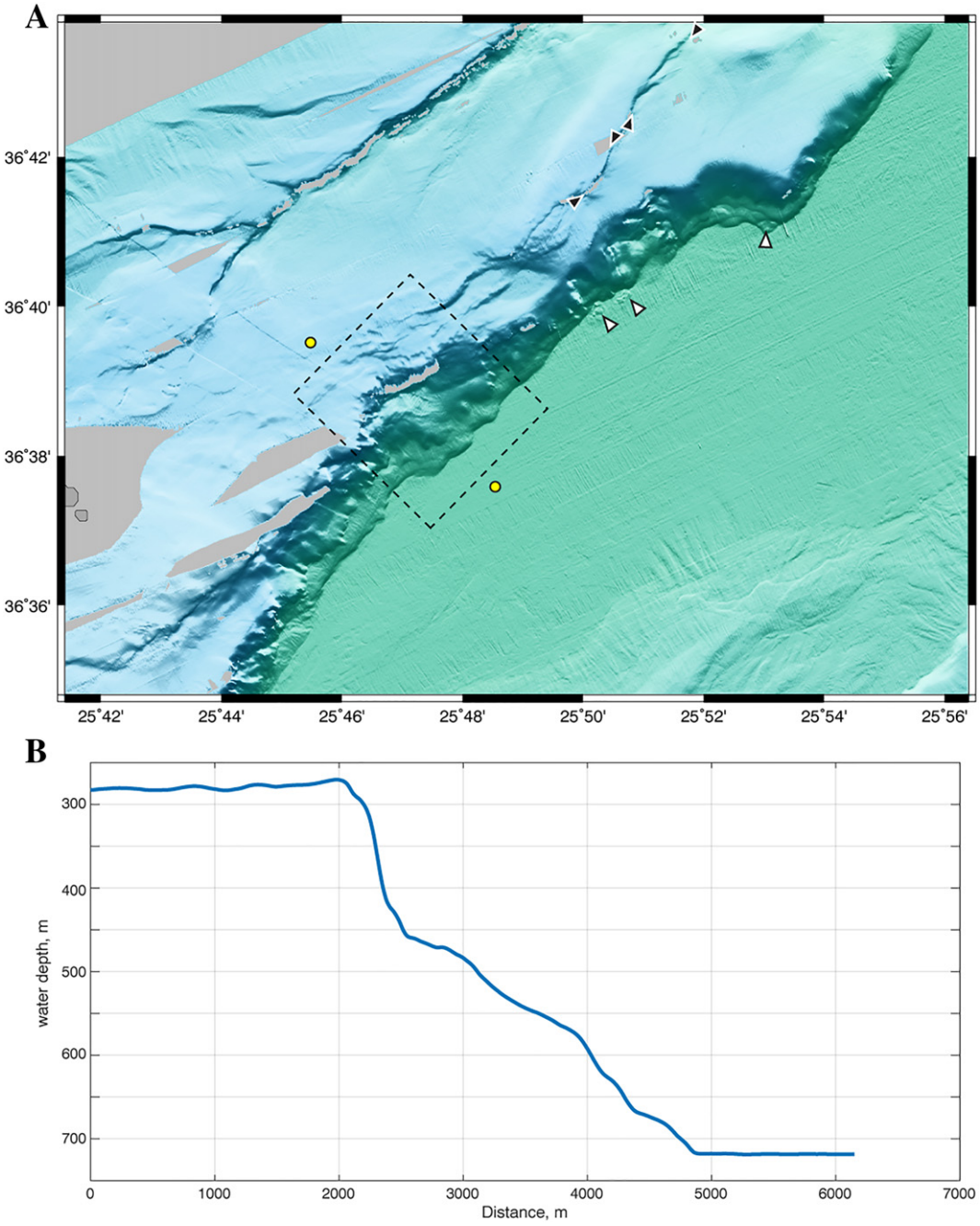

Fig. 11. Large landslide along the center of the Santorini-Amorgos Fault. (a) Bathymetric map illuminated from the north from the R/V *Langseth* data, color scale as in Fig. 2. Note the large lobate landslide (dashed box) as well as recent seafloor deposits along the northern portion of the base of the fault scarp (white arrows). Note the sharpness of the Amorgos Fault in the northwestern part of the map. Secondary normal faults (black arrows) cut the relay ramp (RR) between these two faults. (b) Profile through the landslide; the end points of the profile are shown by yellow dots in (a). The headwall scarp has a slope of 35%, while the landslide toe has a slope of ~13%. (For interpretation of the references to color in this figure legend, the reader is referred to the web version of this article.)

This young wrinkled layer is widespread and drapes the volcano's flanks where its thickness and extent are shaped by preexisting topography; the details of the depositional pattern can be inferred from our merged swath maps (Figs. 2 & 3). It is thickest in the preexisting marine canyon on the SW flank of the island (Fig. 7b) (Sigurdsson et al., 2006), diverges away from seafloor ridges radiating out from Santorini, and is banked up against the shallow topography of the Ios and Anafi Faults (Fig. 3). On the central west coast the flow is diverted to the south when it impinges on the preexisting topography of the island of Christiana and the three underwater volcanic domes (black arrows Fig. 7b). No particular interaction of the flows with Kolumbo volcano can be discerned likely because of overprinting of the seafloor morphology by more recent eruptive episodes at Kolumbo volcano (Hübscher et al., 2015) (Figs. 1–3). Interestingly to the west the most distal portions of the wrinkled surface (with NW-SE wrinkles at this location) appears to be overlain by cross cutting ripples that are oriented NNE-SSW (black arrows Fig. 7a). The origin of these deep water cross-cutting features is likely also related to the deposition of water sediments as a result of roughly east-west bottom currents in the Christiana Basin, consistent with our inference for the interaction of sediments with the Proteus Knoll. This northwestern flow also shows evidence of a number of small pockets of secondary downslope mass wasting (white arrows

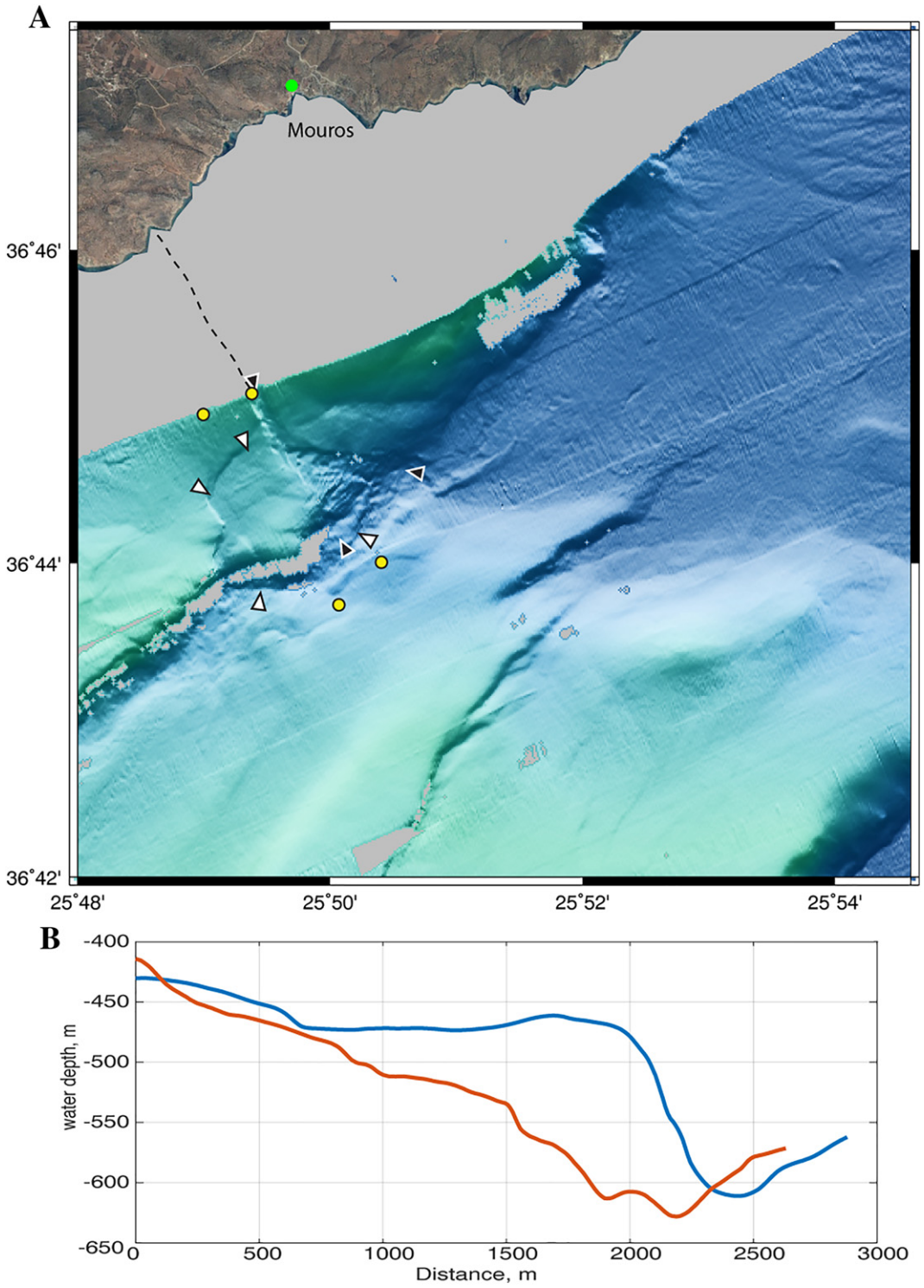

Fig. 12. Small landslide and debris chute on the Amorgos Fault. (a) Bathymetric map illuminated from the north from the R/V *Langseth* data, color scale as in Fig. 2. The landslide has a concave headwall scarp and convex toe (white arrows). The debris chute (black arrows) connects a triangular bay on the south coast of Amorgos (dashed line and Google Earth overlay) with the eastern margin of this landslide. Mouros Bay (green dot) experienced unusually high runups (20 m) during the local tsunami in 1956 (Okal et al., 2009) (b) Profiles through the landslide (blue) and debris chute (red) – end points of the profiles are shown as yellow dots on the map (a). (For interpretation of the references to color in this figure legend, the reader is referred to the web version of this article.)

Fig. 7a). Thus while influenced by existing topography, the pyroclastic flows have significantly shaped the seafloor immediately around Santorini. Yet this topography continues to be reshaped by mass wasting (Croff Bell et al., 2013) and volcanism.

5.4. Submarine landslides

In this section we discuss two newly discovered submarine landslides: those on the Santorini-Amorgos and Amorgos faults. These two

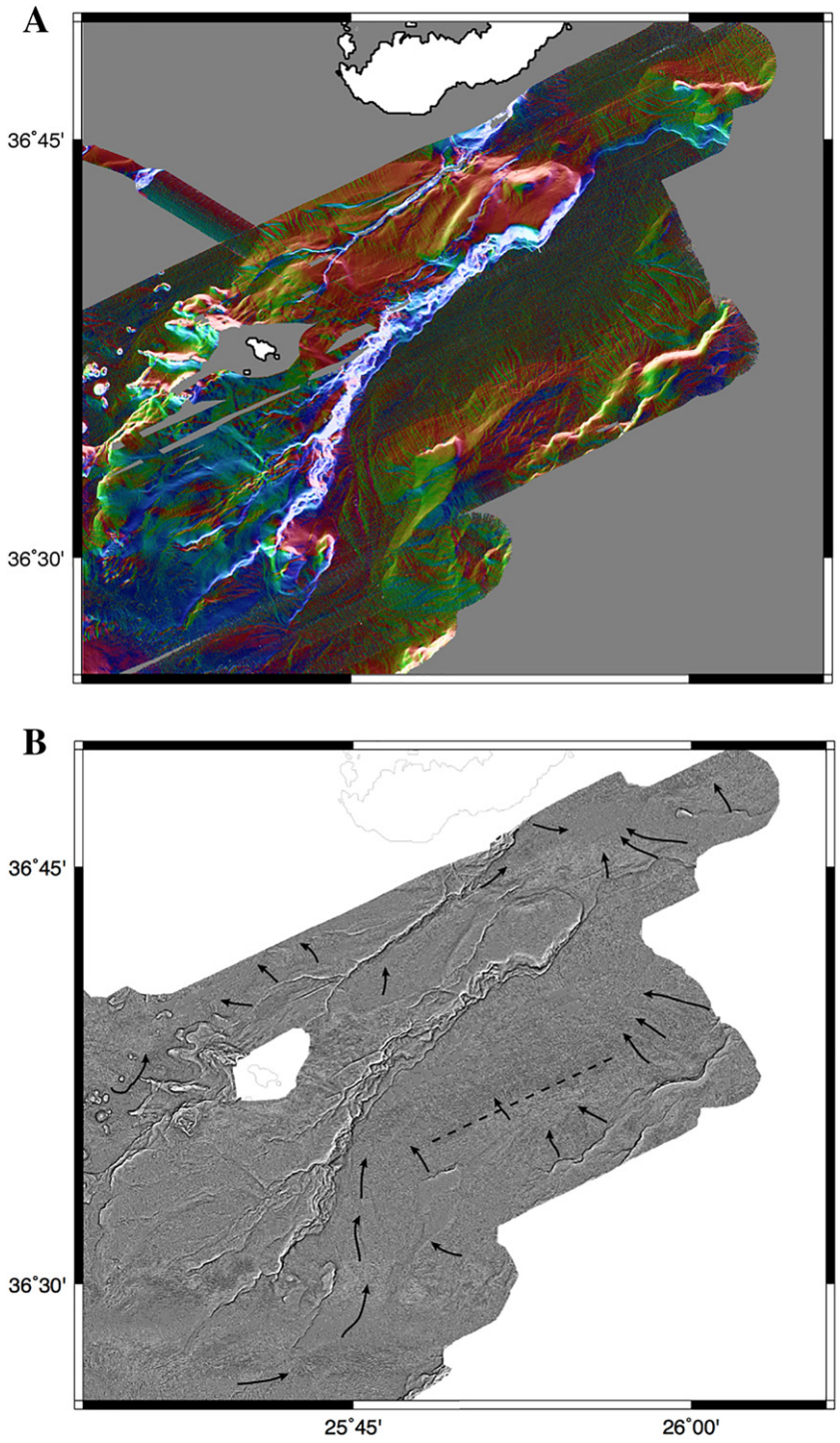

Fig. 13. Seafloor channels in the Anafi basin. (a) Color map of slope azimuth highlighted in white by slope magnitude calculated from the R/V *Langseth* map. (b) Profile curvature for the merged map showing the inferred flow direction of sediment-laden waters (arrows) and the location of the Knudsen profile in Fig. 14 (dashed line).

large and recently active normal faults are subject to mass wasting in response to topography generated by ongoing tectonism. This mass wasting may simply result from over steepening of slopes or be triggered by earthquake induced ground shaking (Wright & Rathje, 2003).

Of particular note is the large submarine landslide on the Santorini-Amorgos Fault (dashed box on Fig. 11). The age of this landslide is uncertain but there is little evidence for rough fresh surfaces, though the steep slopes do not allow detailed probing of the surface with the Knudsen subbottom profiler. Submersible investigation of this feature would help resolve this question, which is of particular interest given that the large tsunami runups that accompanied the 1956 earthquakes are thought to be due to a submarine landslide triggered by this earthquake (Okal et al., 2009). However the volume estimate for the landslide, ~1 km^3, is likely too small; it comprises only 20% of the 5 km^3 required at roughly the same distance from the shore in the tsunami modeling of Okal et al. (2009).

Another possible source for the localized tsunami runup that accompanied the 1956 earthquake is the smaller (~0.3 km^3) submarine landslide on the seaward extension of the Amorgos Fault (Fig. 12). The overlying narrow debris channel indicates ongoing mass movement in this area. While smaller in volume this landslide is located very close to the south coast of Amorgos where tsunami runup in 1956 was the

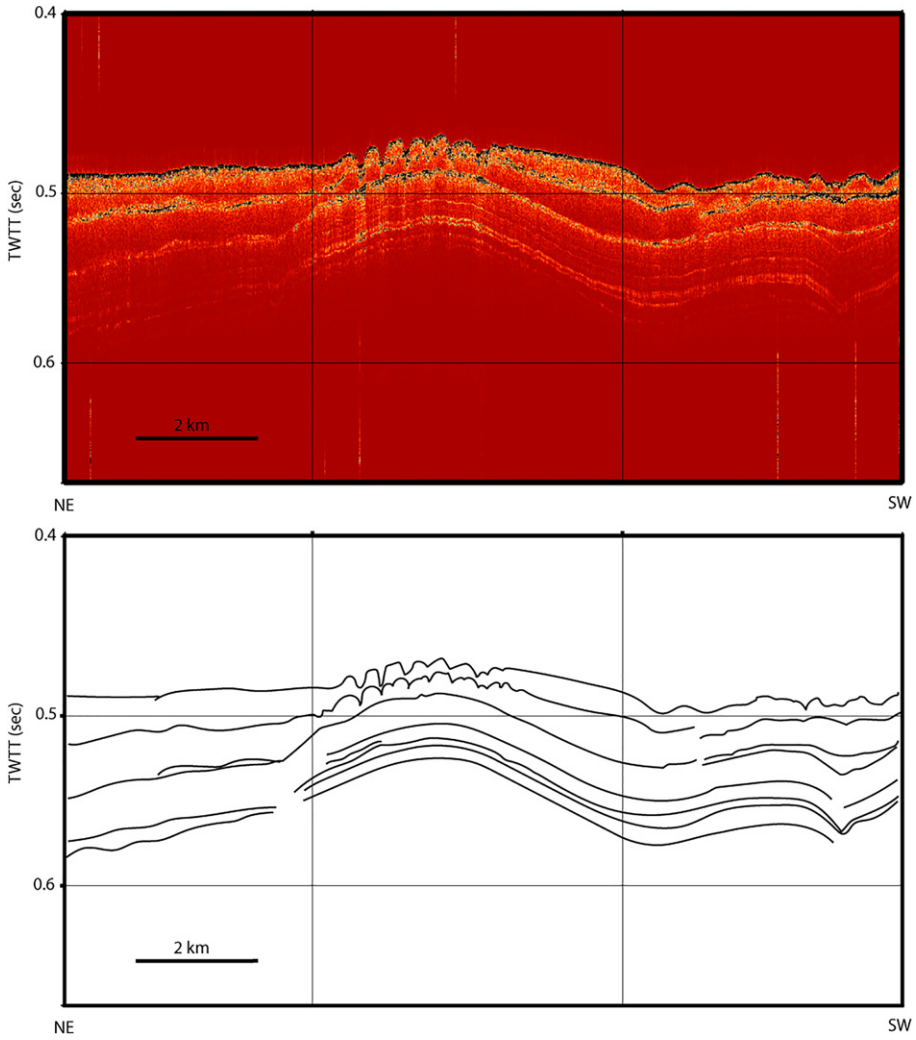

Fig. 14. Knudsen subbottom echosounder profile through four parallel channels in the central Amorgos Basin. (a) Echosounder data along the profile shown by the dashed line in Fig. 13. (b) Line drawing of the seismic facies in (a). Note the very recent development of these channels, which are located on a local high in the subsurface.

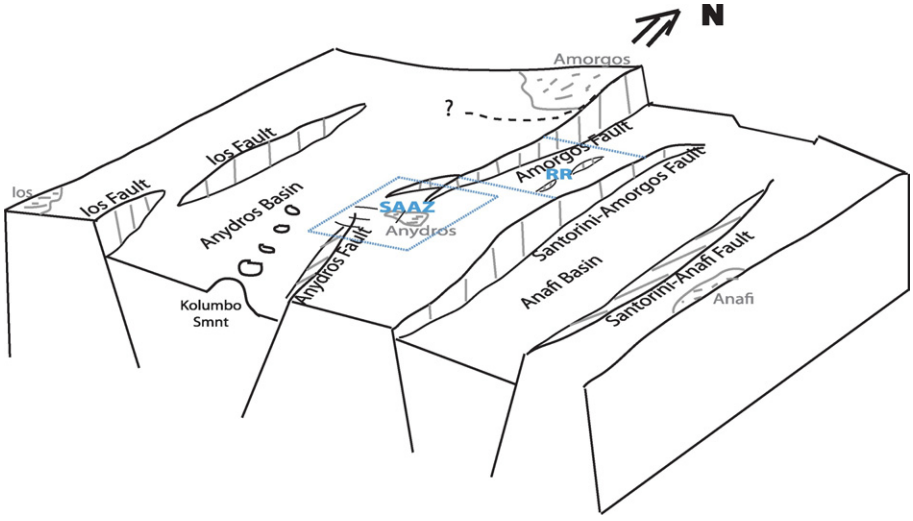

Fig. 15. Sketch of seafloor basins, normal faults, and their interactions between the islands of Santorini and Amorgos. The Santorini-Anafi and Santorini-Amorgos Faults bound the Anafi Basin. The Anydros Fault and the Ios Fault to the north bound the Anydros Basin, which hosts the Kolumbo seamount and volcanic chain. The Anydros Horst lies between the Santorini-Amorgos Fault and the Anydros Fault. Where the south-dipping Santorini-Amorgos and Amorgos faults overlap a synthetic accommodation zone forms a left-stepping relay ramp (blue dashed lines around region RR) with internal fractures. In contrast at the southern extension of the Amorgos Fault there is a change of polarity to the Anydros Fault. This geometry results in a synclinal antithetic accommodation zone (blue dashed box around region SAAZ); the resulting deformation zone lifts the island of Anydros above sea level and may be the source of the continuous low seismicity levels around Anydros as well as of the complex of small faults in this region. (For interpretation of the references to color in this figure legend, the reader is referred to the web version of this article.)

greatest (Okal et al., 2009). Indeed the headwall of the landslide is located 4 km almost directly south (190°) of Mouros Bay, where the largest 20 m local tsunami runup was observed (site 6 in Okal et al. (2009)). The proximity of the landslide to the coast could explain why the runup was so localized. Furthermore, failure downslope to the south is consistent with initial downdraw observed at the Mouros site (Okal et al., 2009). Tsunami modeling is needed to confirm whether displacement of this volume close to shore can generate the required run-up magnitudes and spatial pattern.

6. Conclusions

1. The seafloor morphology around Santorini in the central Aegean backarc of the Hellenic subduction zone is shaped by the interactions between backarc extension, arc volcanism, and mass wasting. These processes are driven by focused northwest-southeast extension as the southeastern Aegean moves away from the Attico-Cycladic complex in response to slab breakup and rollback.
2. The new merged high-resolution swath map together with Knudsen subbottom echosounder profiles reveal that changes in seafloor topography and accompanying mass wasting are more prevalent in the Amorgos-Anydros-Anafi region to the east of Santorini than in the Christiana Basin to the west. This indicates that recent tectonic deformation is concentrated in the Amorgos- Anydros-Anafi area consistent with complex faulting and historically elevated seismicity in that region.
3. We delineate the interactions of the large normal faults between the island of Amorgos and Santorini – the region of the largest 20th century earthquake in Greece (Fig. 15). The large opposing inward facing normal faults give rise to the Anydros and Amorgos Basins. The interactions between the terminations of these fault segments explains the complex faulting structures seen around the island of Anydros. A large relay ramp north of Anydros transfers motion from the Amorgos Fault to the Santorini-Amorgos Fault. The change in polarity between the end of the Amorgos Fault and the Anydros Fault forms a synclinal antithetic accommodation zone (SAAZ) that lifts Anydros island above sea level and generates the complex of faults and accompanying microseismicity in this region (Bohnhoff et al., 2006).
4. Recent volcanism is focused northeast of Santorini consistent with recent faulting and deformation generating pathways in the lithosphere that allow magma to rise. We identify new volcanic features both in the Anydros Basin and the Christiana Basin. Volcanic constructs along the Kolumbo volcanic chain extend further to the NE than was known (23 volcanic cones compared to 19 identified previously (Nomikou et al., 2012)). We also discovered a new volcanic feature (Proteus Knoll) and nearby buried edifice in the NW portion of the Christiana Basin – the nature of the Proteus Knoll (age and composition) and its localization are enigmatic. There is no evidence of tectonic focusing of volcanism, however this edifice does lie on the curving volcanic arc line between Santorini and Milos.
5. Submarine landsliding features along the Santorini-Amorgos and Amorgos Faults suggest that tsunamis from mass wasting events occur in the region and could be triggered by ground shaking due to nearby earthquakes or volcanic eruptions as well as by nearby coastal erosion.
6. Seafloor morphology around Santorini is dominated by features formed during, and immediately after, the Late Bronze Age eruption such as the northern caldera entrance channel and the wrinkled seafloor pyroclastic flow deposits. Subsequently multistage submarine landsliding on the southeast side of the volcano has modified this flank while secondary mass wasting has an ongoing smaller-scale effect throughout the area.

Supplementary data to this article can be found online at http://dx.doi.org/10.1016/j.tecto.2017.06.005.

Acknowledgements

This manuscript benefitted from the comments of two anonymous reviewers and the Editor in Chief, Rob Govers, and from discussions with Ray Weldon, Josh Roering, Dave Furbish, and Javier Escartín. We thank the ship captain and crew and science officers of the R/V *Marcus Langseth* for their indispensable contribution to collecting this dataset. For the data processing, vizualisation, and maps we used the freely available software packages MBsystem, GMT, and OpendTect. This work was supported by US National Science Foundation grant number OCE-1459794.

References

Ambraseys, N.N., 1960. The seismic sea wave of July 9, 1956, in the Greek archipelago. J. Geophys. Res. 65 (4), 1257–1265.
Bohnhoff, M., Rische, M., Meier, T., 2004. CYC-NET: a temporary seismic network on the Cyclades (Aegean Sea, Greece). Seismol. Res. Lett. 75 (3), 352–359.
Bohnhoff, M., Rische, M., Meier, T., Becker, D., 2006. Microseismic activity in the Hellenic Volcanic Arc, Greece, with emphasis on the seismotectonic setting of the Santorini–Amorgos zone. Tectonophysics 423:17–33. http://dx.doi.org/10.1016/j.tecto.2006.03.024.
Bozkurt, E., Sözbilir, H., 2006. Evolution of the large-scale active Manisa Fault, Southwest Turkey: implications on fault development and regional tectonics. Geodin. Acta 19 (6), 427–453.
Brüstle, A., Friederich, W., Meier, T., Gross, C., 2014. Focal mechanism and depth of the 1956 Amorgos twin earthquakes from waveform matching of analogue seismograms. Solid Earth 5:1027–1044. http://dx.doi.org/10.5194/se-5-1027-2014.
Carey, S., Sigurdsson, H., 2000. Volcanic hazards from pyroclastic flow discharge into the sea: examples from the 1883 eruption of Krakatau, Indonesia. Geol. Soc. Am. Spec. Pap. 345:1–14. http://dx.doi.org/10.1130/0-8137-2345-0.1.
Carey, S., Sigurdsson, H., Mandeville, C., Bronto, S., 1996. Pyroclastic flows and surges over water: an example from the 1883 Krakatau eruption. Bull. Volcanol. 57:493–511. http://dx.doi.org/10.1007/BF00304435.
Carlson, R.L., Melia, P.J., 1984. Subduction hinge migration. Tectonophysics 102:399–411. http://dx.doi.org/10.1016/0040-1951(84)90024-6.
Comninakis, P.E., Papazachos, B.C., 1986. A Catalogue of Earthquakes in Greece and the surrounding Area for the Period 1901–1985. Publ. Lab., Univ. of Thessaloniki.
Courtillot, V., 1982. Propagating rifts and continental breakup. Tectonics 1 (3):239–250. http://dx.doi.org/10.1029/TC001i003p00239.
Croff Bell, K.L., Carey, S.N., Nomikou, P., Sigurdsson, H., 2013. Submarine evidence of a debris avalanche deposit on the eastern slope of Santorini volcano, Greece. Tectonophysics 597-598:147–160. http://dx.doi.org/10.1016/j.tecto.2012.05.006.
Dermitzakis, D.M., Papanikolaou, D.J., 1981. Paleogeography and geodynamics of the Aegean region during the Neogene. Ann. Géol. Pays Hellén. 30, 245–289.
Dewey, J.F., Pitman, W.C., Ryan, W., 1973. Plate tectonics and the evolution of the Alpine system. Geol. Soc. Am. Bull. 84, 3137–3180.
Dimitriadis, I., Karagianni, E., Panagiotopoulos, D., Papazachos, C., Hatzidimitriou, P., Bohnhoff, M., Rische, M., Meier, T., 2009. Seismicity and active tectonics at Coloumbo Reef (Aegean Sea, Greece): monitoring an active volcano at Santorini Volcanic Center using a temporary seismic network. Tectonophysics 465 (1–4):136–149. http://dx.doi.org/10.1016/j.tecto.2008.11.005.
Dominey-Howes, D., 2004. A re-analysis of the Late Bronze Age eruption and tsunami of Santorini, Greece, and the implications for the volcano–tsunami hazard. J. Volcanol. Geotherm. Res. 130:107–132. http://dx.doi.org/10.1016/S0377-0273(03)00284-1.
Dominey-Howes, D., Papadopoulos, G.A., Dawson, A.G., 2000. Geological and historical investigation of the 1650 Mt. Columbo (Thera Island) eruption and tsunami, Aegean Sea, Greece. Nat. Hazards 21 (1):83–96. http://dx.doi.org/10.1023/A:1008178100633.
Druitt, T.H., 2014. New insights into the initiation and venting of the Bronze-Age eruption of Santorini (Greece), from component analysis. Bull. Volcanol. 76 (2):794. http://dx.doi.org/10.1007/s00445-014-0794-x.
Druitt, T.H., Francaviglia, V., 1992. Caldera formation on Santorini and the physiography of the islands in the late Bronze Age. Bull. Volcanol. 54:484–493. http://dx.doi.org/10.1007/BF00301394.
Druitt, T.H., Edwards, L., Mellors, R.M., Pyle, D.M., Sparks, R.S.J., Lanphere, M., Davies, M., Barreiro, B., 1999. Santorini volcano. Geol. Soc. Spec. Mem. 19 (165 p).
Endrun, B., Meier, T., Lebedev, S., Bohnhoff, M., Stavrakakis, G., Harjes, H.-P., 2008. Svelocity structure and radial anisotropy in the Aegean region from surface wave dispersion. Geophys. J. Int. 174 (2):593–616. http://dx.doi.org/10.1111/j.1365-246X.2008.03802.x.
Faccenna, C., Bellier, O., Martinod, J., Piromallo, C., 2006. Slab detachment beneath eastern Anatolia: a possible cause for the formation of the North Anatolian fault. Earth Planet. Sci. Lett. 242:85–97. http://dx.doi.org/10.1029/2001JB001690.
Faulds, J.E., Varga, R.J., 1998. The role of accommodation zones and transfer zones in the regional segmentation of extended terranes. Geol. Soc. Am. Spec. Pap. 323.
Feuillet, N., 2013. The 2011–2012 unrest at Santorini rift: stress interaction between active faulting and volcanism. Geophys. Res. Lett. 40 (14), 3532–3537.
Floyd, M.A., Billiris, H., Paradissis, D., Veis, G., 2010. A new velocity field for Greece: implications for the kinematics and dynamics of the Aegean. J. Geophys. Res. 115 (B10403). http://dx.doi.org/10.1029/2009JB007040.
Fossen, H., Rotevatn, A., 2016. Fault linkage and relay structures in extensional settings—a review. Earth Sci. Rev. 154:14–28. http://dx.doi.org/10.1016/j.earscirev.2015.11.014.

Friederich, W., Brüstle, A., Küperkoch, L., Meier, T., Lamara, S., E. Working Group, 2014. Focal mechanisms in the southern Aegean from temporary seismic networks; implications for the regional stress field and ongoing deformation processes. Solid Earth 5 (1):275–297. http://dx.doi.org/10.5194/se-5-275-2014.

Friedrich, W.L., 2006. Santorini eruption radiocarbon dated to 1627–1600 B.C. Science 312 (5773):548. http://dx.doi.org/10.1126/science.1125087.

Fytikas, M., Innocenti, F., Manetti, P., Peccerillo, A., Mazzuoli, R., Villari, L., 1984. Tertiary to Quaternary evolution of volcanism in the Aegean region. Geol. Soc. Lond. Spec. Publ. 17 (1):687–699. http://dx.doi.org/10.1144/GSL.SP.1984.017.01.55.

Galanopoulos, A., 1956. Seismological Institute Bulletin 1955, Publ. No, 6, Athens.

Galanopoulos, A.G., 1960. Tsunamis observed on the coasts of Greece from antiquity to present time. Ann. Geofis. 30, 369–386.

Gautier, P., Brun, J.-P., 1994. Crustal-scale geometry and kinematics of late-orogenic extension in the central Aegean (Cyclades and Ewia Island). Tectonophysics 238: 399–424. http://dx.doi.org/10.1016/0040-1951(94)90066-3.

Gautier, P., Brun, J.P., Moriceau, R., Sokoutis, D., Martinod, J., 1999. Timing, kinematics and cause of Aegean extension: a scenario based on a comparison with simple analogue experiments. Tectonophysics 315, 31–72.

Heiken, G., McCoy, F., 1984. Caldera development during the Minoan eruption, Thira, Cyclades, Greece. J. Geophys. Res. 89:8441–8462. http://dx.doi.org/10.1029/JB089iB10p08441.

Hübscher, C., Ruhnau, M., Nomikou, P., 2015. Volcano-tectonic evolution of the polygenetic Kolumbo submarine volcano/Santorini (Aegean Sea). J. Volcanol. Geotherm. Res. 291:101–111. http://dx.doi.org/10.1016/j.jvolgeores.2014.12.020.

Huijsmans, J., Barton, M., Salters, V., 1988. Geochemistry and evolution of the calc-alkaline volcanic complex of Santorini, Aegean Sea, Greece. J. Volcanol. Geotherm. Res. 34, 283–306.

Johnston, E.N., Sparks, R.S.J., Nomikou, P., Livanos, I., Carey, S., Phillips, J.C., Sigurdsson, H., 2015. Stratigraphic relations of Santorini's intracaldera fill and implications for the rate of post-caldera volcanism. J. Geol. Soc. Lond. 172 (3):323–335. http://dx.doi.org/10.1144/jgs2013-114.

Jolivet, L., Faccenna, C., Huet, B., Labrousse, L., Le Pourhiet, L., Lacombe, O., Lecomte, E., Burov, E., Denèle, Y., Brun, J.-P., Philippon, M., Paul, A., Salaün, G., Karabulut, H., Piromallo, C., Monié, P., Gueydan, F., Okay, A.I., Oberhänsli, R., Pourteau, A., Augier, R., Gadenne, L., Driussi, O., 2013. Aegean tectonics: strain localisation, slab tearing and trench retreat. Tectonophysics 597-598 (C):1–33. http://dx.doi.org/10.1016/j.tecto.2012.06.011.

Karagianni, E.E., Papazachos, C.B., 2007. Shear velocity structure in the Aegean region obtained by joint inversion of Rayleigh and Love waves. Geol. Soc. Lond. Spec. Publ. 291 (1):159–181. http://dx.doi.org/10.1144/SP291.8.

Keller, J., Rehren, T., Stadlbauer, E., 1990. Explosive volcanism in the Hellenic Arc: a summary and review. Thera and the Aegean World III. 2, pp. 13–26.

Kokkalas, S., Aydin, A., 2013. Is there a link between faulting and magmatism in the south-central Aegean Sea? Geol. Mag. 150:193–224. http://dx.doi.org/10.1017/S0016756812000453.

Konstantinou, K.I., 2010. Crustal rheology of the Santorini-Amorgos zone: implications for the nucleation depth and rupture extent of the 9 July, 1956 Amorgos earthquake, southern Aegean. J. Geodyn. 50:400–409. http://dx.doi.org/10.1016/j.jog.2010.05.002.

Kvalstad, T.J., Andresen, L., Forsberg, C.F., Berg, K., 2005. The Storegga slide: evaluation of triggering sources and slide mechanics. Mar. Pet. Geol. 22:245–256. http://dx.doi.org/10.1016/j.marpetgeo.2004.10.019.

Le Pichon, X., Angelier, J., 1979. The Hellenic arc and trench system: a key to the neotectonic evolution of the eastern Mediterranean area. Tectonophysics 60:1–42. http://dx.doi.org/10.1016/0040-1951(79)90131-8.

Le Pichon, X., Kreemer, C., 2010. The Miocene-to-present kinematic evolution of the Eastern Mediterranean and Middle East and its implications for dynamics. Annu. Rev. Earth Planet. Sci. 38 (1):323–351. http://dx.doi.org/10.1146/annurev-earth-040809-152419.

Makris, J., 1978. The crust and upper mantle of the Aegean region from deep seismic soundings. Tectonophysics 46 (3–4):269–284. http://dx.doi.org/10.1016/0040-1951(78)90207-X.

Makropoulos, K.C., Drakopoulos, J.K., Latousakis, J.B., 1989. A revised and extended earthquake catalogue for Greece since 1900. Geophys. J. Int. 98 (2):391–394. http://dx.doi.org/10.1111/j.1365-246X.1989.tb03360.x.

Marinatos, S., 1939. The volcanic destruction of Minoan Crete. Antiquity 13 (52):425–439. http://dx.doi.org/10.1017/S0003598X00028088.

Mascle, J., Martin, L., 1990. Shallow structure and recent evolution of the Aegean Sea: a synthesis based on continuous reflection profiles. Mar. Geol. 94 (4):271–299. http://dx.doi.org/10.1016/0025-3227(90)90060-W.

Masson, D.G., Harbitz, C.B., Wynn, R.B., Pedersen, G., Løvholt, F., 2006. Submarine landslides: processes, triggers and hazard prediction. Phil. Trans. R. Soc. London 364 (1845):2009–2039. http://dx.doi.org/10.1098/rsta.2006.1810.

McClusky, S., Balassanian, S., Barka, A., 2000. Global positioning system constraints on plate kinematics and dynamics in the eastern Mediterranean and Caucasus. J. Geophys. Res. 105:5695–5719. http://dx.doi.org/10.1029/1999JB900351.

McKenzie, D., 1972. Active tectonics of the Mediterranean region. Geophys. J. R. Astron. Soc. 30 (2):109–185. http://dx.doi.org/10.1111/j.1365-246X.1972.tb02351.x.

Mitchell, N.C., Masson, D.G., Watts, A.B., Gee, M.J.R., Urgeles, R., 2002. The morphology of the submarine flanks of volcanic ocean islands. J. Volcanol. Geotherm. Res. 115 (1–2): 83–107. http://dx.doi.org/10.1016/S0377-0273(01)00310-9.

Ninkovich, D., Hays, J.D., 1972. Mediterranean island arcs and origin of high potash volcanoes. Earth Planet. Sci. Lett. 16, 331–345.

Nomikou, P., Carey, S., Papanikolaou, D., Bell, K.C., 2012. Submarine volcanoes of the Kolumbo volcanic zone NE of Santorini Caldera, Greece. Glob. Planet. Chang. 90-91: 135–151. http://dx.doi.org/10.1016/j.gloplacha.2012.01.001.

Nomikou, P., Papanikolaou, D., Alexandri, M., Sakellariou, D., Rousakis, G., 2013. Submarine volcanoes along the Aegean volcanic arc. Tectonophysics 597:123–146. http://dx.doi.org/10.1016/j.tecto.2012.10.001.

Nomikou, P., Parks, M.M., Papanikolaou, D., Pyle, D.M., Mather, T.A., Carey, S., Watts, A.B., Paulatto, M., Kalnins, M.L., Livanos, I., Bejelou, K., Simou, E., Perros, 2014. The emergence and growth of a submarine volcano: the Kameni islands, Santorini (Greece). Geogr. Res. (J. Inst. Aust. Geogr.) 1-2 (C):8–18. http://dx.doi.org/10.1016/j.grj.2014.02.002.

Nomikou, P., Druitt, T.H., Hubscher, C., Mather, T.A., Paulatto, M., Kalnins, L.M., Kelfoun, K., Papanikolaou, D., Bejelou, K., Lampridou, D., Pyle, D.M., Carey, S., Watts, A.B., Weiß, B., Parks, M.M., 2016a. Post-eruptive flooding of Santorini caldera (Greece), and implications for tsunami generation. Nat. Commun. 7:1–22. http://dx.doi.org/10.1038/ncomms13.

Nomikou, P., Hübscher, C., Ruhnau, M., bejelou, K., 2016b. Tectono-stratigraphic evolution through successive extensional events of the Anydros Basin, hosting Kolumbo volcanic field at the Aegean Sea, Greece. Tectonophysics 671:202–217. http://dx.doi.org/10.1016/j.tecto.2016.01.021.

Nyst, M., 2004. New constraints on the active tectonic deformation of the Aegean. J. Geophys. Res. 109 (B11), B11406. http://dx.doi.org/10.1029/2003jb002830.

Okal, E.A., Synolakis, C.E., Uslu, B., Kalligeris, N., Voukouvalas, E., 2009. The 1956 earthquake and tsunami in Amorgos, Greece. Geophys. J. Int. 178 (3):1533–1554. http://dx.doi.org/10.1111/j.1365-246X.2009.04237.x.

Papadopoulos, G., 2015. Tsunamis in the European-Mediterranean Region: From Historical Record to Risk Mitigation. Elsevier.

Papadopoulos, G.A., Pavlides, S.B., 1992. The large 1956 earthquake in the South Aegean: macroseismic field configuration, faulting, and neotectonics of Amorgos Island. Earth Planet. Sci. Lett. 113, 383–396.

Papadopoulos, G.A., Kondopoulou, D.P., Leventakis, G.A., Pavlides, S.B., 1986. Seismotectonics of the Aegean region. Tectonophysics 124 (1–2):67–84. http://dx.doi.org/10.1016/0040-1951(86)90138-1.

Papanikolaou, D., 2009. Timing of tectonic emplacement of the ophiolites and terrane paleogeography in the Hellenides. Lithos 108, 262–280.

Papanikolaou, D., 2013. Tectonostratigraphic models of the Alpine terranes and subduction history of the Hellenides. Tectonophysics 595-596:1–24. http://dx.doi.org/10.1016/j.tecto.2012.08.008.

Papanikolaou, D.J., Royden, L.H., 2007. Disruption of the Hellenic arc: Late Miocene extensional detachment faults and steep Pliocene-Quaternary normal faults—or what happened at Corinth? Tectonics http://dx.doi.org/10.1029/2006TC002007.

Papazachos, B.C., 1980. Seismicity rates and long-term earthquake prediction in the Aegean area. Quaterniones Geodaesiae 3, 171–190.

Papazachos, B.C., 1990. Seismicity of the Aegean and surrounding area. Tectonophysics 178:287–308. http://dx.doi.org/10.1016/0040-1951(90)90155-2.

Papazachos, B.C., Delibasis, N.D., 1969. Tectonic stress field and seismic faulting in the area of Greece. Tectonophysics 7 (3):231–255. http://dx.doi.org/10.1016/0040-1951(69)90069-9.

Papazachos, C., Nolet, G., 1997. P and S deep velocity structure of the Hellenic area obtained by robust nonlinear inversion of travel times. J. Geophys. Res. 102 (B4): 8349–8367. http://dx.doi.org/10.1029/96JB03730.

Papazachos, B.C., Panagiotopoulos, D.G., 1993. Normal faults associated with volcanic activity arc. Tectonophysics 220 (1–4):301–308. http://dx.doi.org/10.1016/0040-1951(93)90237-E.

Pe-Piper, G., Piper, D., 2007. Neogene backarc volcanism of the Aegean: new insights into the relationship between magmatism and tectonics. Geol. Soc. Am. Spec. Pap. 418. http://dx.doi.org/10.1130/2007.2418(02).

Perissoratis, C., 1995. The Santorini volcanic complex and its relation to the stratigraphy and structure of the Aegean arc, Greece. Mar. Geol. 128 (1–2):37–58. http://dx.doi.org/10.1016/0025-3227(95)00090-L.

Perissoratis, C., Papadopoulos, G., 1999. Sediment instability and slumping in the southern Aegean Sea and the case history of the 1956 tsunami. Mar. Geol. 161, 287–305.

Piper, D.J.W., Perissoratis, C., 2003. Quaternary neotectonics of the South Aegean arc. Mar. Geol. 198 (3–4):259–288. http://dx.doi.org/10.1016/S0025-3227(03)00118-X.

Piper, D., Pe-Piper, G., Perissoratis, C., 2007. Distribution and chronology of submarine volcanic rocks around Santorini and their relationship to faulting. Geol. Soc. Lond. Spec. Publ. 291:99–111. http://dx.doi.org/10.1144/SP291.5.

Reilinger, R., McClusky, S., Paradissis, D., Ergintav, S., Vernant, P., 2010. Geodetic constraints on the tectonic evolution of the Aegean region and strain accumulation along the Hellenic subduction zone. Tectonophysics 488 (1–4):22–30. http://dx.doi.org/10.1016/j.tecto.2009.05.027.

Rosendahl, B.R., 1987. Architecture of continental rifts with special reference to East Africa. Annu. Rev. Earth and Planetary Science Letters 15, 445–503.

Royden, L.H., Papanikolaou, D.J., 2011. Slab segmentation and late Cenozoic disruption of the Hellenic arc. Geochem. Geophys. Geosyst. 12 (3). http://dx.doi.org/10.1029/2010GC003280.

Sachpazi, M., Laigle, M., Charalampakis, M., 2015. Segmented Hellenic slab rollback driving Aegean deformation and seismicity. Geophys. Res. Lett. 1–8. http://dx.doi.org/10.1002/(ISSN)1944-8007.

Sakellariou, D., Sigurdsson, H., Alexandri, M., Carey, S., Rousakis, G., Nomikou, P., Georgiou, P., Ballas, D., 2010. Active tectonics in the Hellenic volcanic arc: the Kolumbo submarine volcanic zone. Bull. Geol. Soc. Greece 43 (2), 1056–1063.

Seward, D., Wagner, G.A., Pichler, H., 1980. Fission track ages of Santorini volcanics (Greece). Thera and the Aegan World II.

Sharp, I.R., Gawthrope, R.L., Underhill, J.R., Gupta, S., 2000. Fault-propagation folding in extensional settings: examples of structural style and syn-rift sedimentary response from the Gulf of Suez rift, Sinai, Egypt. Geol. Soc. Am. Bull. 112:1877–1899. http://dx.doi.org/10.1130/0016-7606(2000)112.

Shaw, B., Jackson, J., 2010. Earthquake mechanisms and active tectonics of the Hellenic subduction zone. Geophys. J. Int. 181:966–984. http://dx.doi.org/10.1111/j.1365-246X.2010.04551.x.

Sigurdsson, H., Carey, S., Alexandri, M., 2006. Marine investigations of Greece's Santorini volcanic field. EOS Trans. Am. Geophys. Union 87, 337–348.

Sodoudi, F., Brüstle, A., Meier, T., Kind, R., Friederich, W., EGELADOS working group, 2015. Receiver function images of the Hellenic subduction zone and comparison to microseismicity. Solid Earth 6 (1):135–151. http://dx.doi.org/10.5194/se-6-135-2015.

Soukis, K., papanikolaou, D., 2004. Contrasting geometry between alpine and late-to post-alpine tectonic structures in Anafi Island (Cyclades). Bull. Geol. Soc. Greece XXXVI, 1688–1696.

Spakman, W., Wortel, M.J.R., Vlaar, N.J., 1988. The Hellenic subduction zone: a tomographic image and its geodynamic implications. Geophys. Res. Lett. 15 (1):60–63. http://dx.doi.org/10.1029/GL015i001p00060.

Stiros, S.C., Marangou, L., Arnold, M., 1994. Quaternary uplift and tilting of Amorgos Island (southern Aegean) and the 1956 earthquake. Earth Planet. Sci. Lett. 128, 65–76.

Taymaz, T., Westaway, R., Reilinger, R., 2004. Active faulting and crustal deformation in the Eastern Mediterranean region. Tectonophysics 391 (1–4):1–9. http://dx.doi.org/10.1016/j.tecto.2004.07.005.

Tirel, C., Gueydan, F., Tiberi, C., Brun, J.-P., 2004. Aegean crustal thickness inferred from gravity inversion. Geodynamical implications. Earth Planet. Sci. Lett. 228 (3–4): 267–280. http://dx.doi.org/10.1016/j.epsl.2004.10.023.

Tsapanos, T.M., Galanopoulos, D., Burton, P.W., 1994. Seismicity in the Hellenic Volcanic Arc: relation between seismic parameters and the geophysical fields in the region. Geophys. J. Int. 117 (3):677–694. http://dx.doi.org/10.1111/j.1365-246X.1994.tb02462.x.

Uyeda, S., Kanamori, H., 1979. Back-arc opening and the mode of subduction. J. Geophys. Res. Solid Earth 84:1049–1061. http://dx.doi.org/10.1029/JB084iB03p01049.

Walcott, C.R., White, S.H., 1998. Constraints on the kinematics of post-orogenic extension imposed by stretching lineations in the Aegean region. Tectonophysics 298, 155–175.

Wallace, L.M., Ellis, S., Mann, P., 2009. Collisional model for rapid fore-arc block rotations, arc curvature, and episodic back-arc rifting in subduction settings. Geochem. Geophys. Geosyst. 10 (5):n/a. http://dx.doi.org/10.1029/2008GC002220.

Wright, S.G., Rathje, E.M., 2003. Triggering mechanisms of slope instability and their relationship to earthquakes and tsunamis. Pure Appl. Geophys. 160 (10−11): 1865–1877. http://dx.doi.org/10.1007/s00024-003-2410-4.

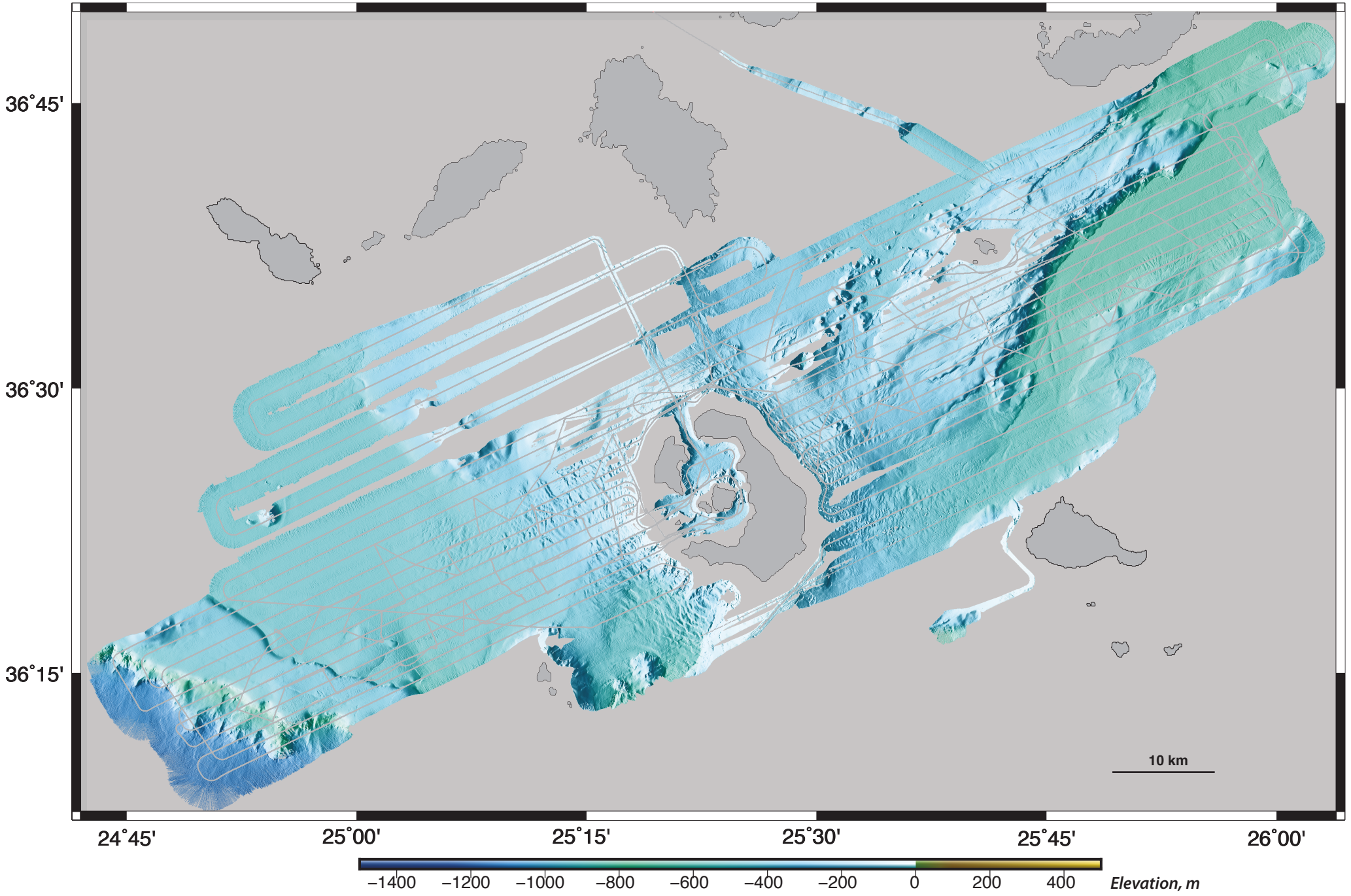

Figure S1. Seafloor bathymetry from R/V *Langseth*. Swath data gridded at 20 m and illuminated from the north. The ship track is shown with grey lines.

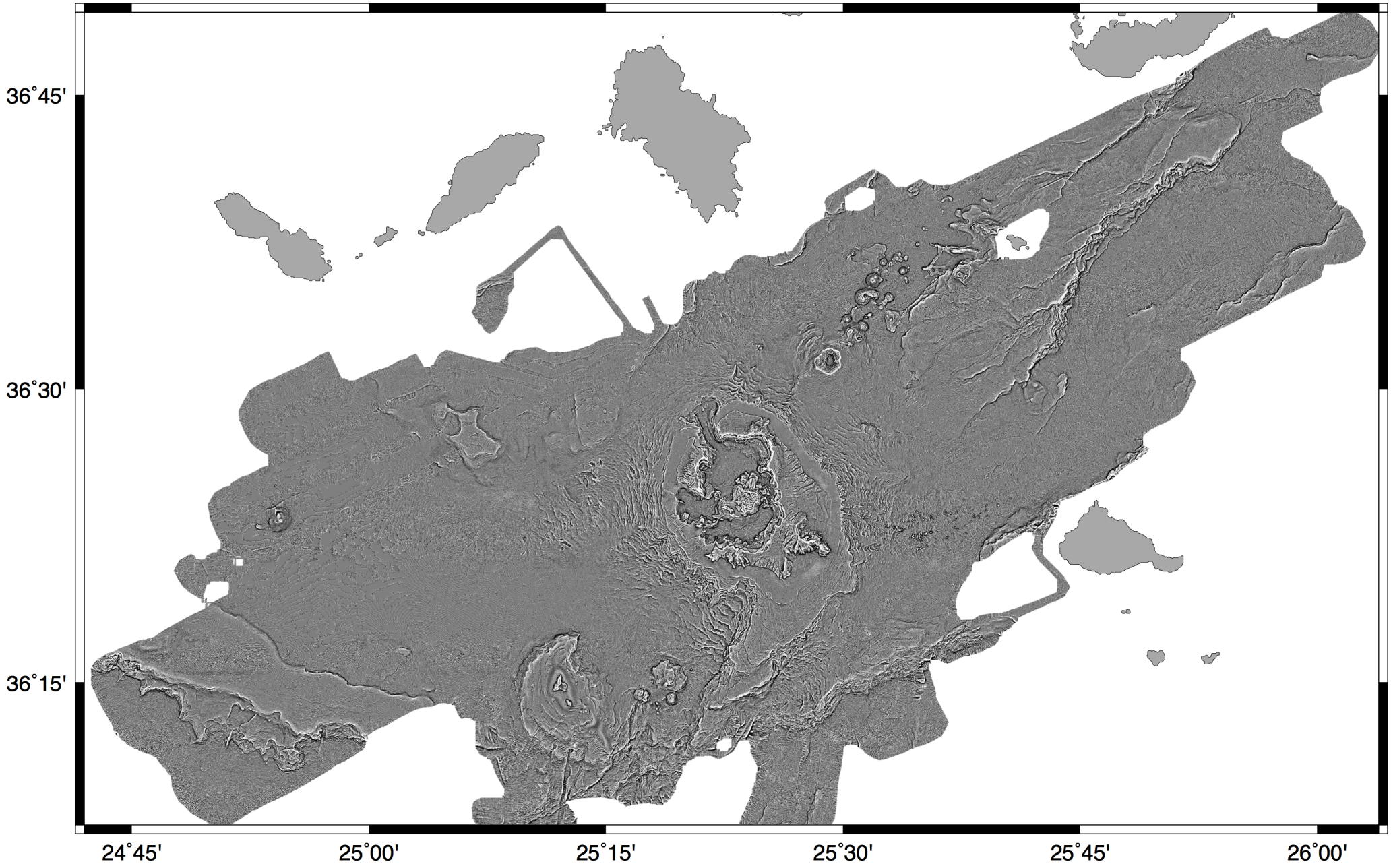

Figure S2. Map of profile curvature calculated from the merged map (Figure 2a). Black and white colors are low and high values of relative profile curvature, respectively.